Resumen

Uno de los fenómenos claves que tienen lugar en la cuba de un reactor de fisión de tipo BWR es la ebullición sub-nucleada. La modelización numérica de este fenómeno todavía está en desarrollo. Por ello, es clave realizar campañas experimentales de ebullición sub-nucleada que sirvan para definir y calibrar los modelos numéricos desarrollados. A este efecto, ABB Corporate Research en Västerås, Suecia, junto con la universidad KTH, realizaron experimentos de ebullición sub-nucleada. El objetivo principal del proyecto es analizar las capacidades que tiene el código libre de dinámica computacional OpenFOAM para reproducir dicho experimento.

En una primera fase del proyecto, se ha estudiado el experimento de ABB y sus resultados. En una segunda fase, se ha profundizado en la fenomenología incluyendo la hidráulica como la transferencia de calor. Posteriormente, el autor se ha familiarizado con el código OpenFOAM.

En cuanto a la modelización numérica del experimento, se ha realizado mediante distintas etapas, aumentando la complejidad del fenómeno a estudiar de forma progresiva, desde la termo-hidráulica sin cambio de fase hasta la ebullición sub-nucleada. En cada caso se ha analizado las hipótesis y simplificaciones necesarias, se han llevado a cabo las simulaciones, los estudios de mallado necesarios y se han extraído las conclusiones pertinentes al comparar los resultados numéricos con los experimentales.

Finalmente, se concluyen las capacidades de OpenFOAM en la simulación de la ebullición sub-nucleada y se aportan ciertas recomendaciones para futuros estudios.

Content

1. Introduction 6
1.1 Aim of the study and objectives 6
1.2 State of the Art 7
2 Experimental set up 7
2.1 Water system 8
2.2 Heaters 8
2.3 Aluminium block 9
2.4 Video recording system 9
2.5 Polycarbonate layer 10
2.6 Insulation 10
3 Phenomenology 10
3.1 Single phase flow 10
3.1.1 Continuity equation 10
3.1.2 Momentum equation 11
3.1.3 Energy equation 11
3.2 Two-fluid model 11
3.2.1 Continuity equation 12
3.2.2 Momentum equation 12
3.2.3 Energy equation 16
3.3 Solid region 16
3.4 Boiling phases 16
4 CFD and OpenFOAM 18
4.1 Computational fluid dynamics (CFD). 18
4.2 OpenFOAM (Open Field Operation And Manipulation). 19
4.3 Single phase solver: chtMultiregionFoam 20
4.3.1 Navier-Stokes algorithm (PIMPLE) 20
4.4 Two phase solvers 21
5 Modelisation of the experiment for the single phase simulation 22
5.1 Simulation simplifications 22
5.2 Geometry and dimensions 24
5.2.1 Axis definition 26
5.3 Mesh 26
5.4 Boundary conditions and numerical strategies 27
5.5 Post-processing procedures 27
5.5.1 Heat through the wall 28

5.5.2 Average outlet temperature....28
5.5.3 Wall temperature values for thermocouple positions....29
5.5.4 Cell and wall values for nucleation sites....29
5.5.5 Sampling setup....31
6 Study 1: single phase flow....33
6.1 Case set up....33
6.1.1 Flow conditions....34
6.1.2 Expected results....35
6.1.3 Q applied to the heaters....35
6.2 Simulation results....36
6.3 Results comparison....38
6.3.1 Outlet water temperature and heat assessment....38
6.3.2 Wall temperature discussion....39
6.3.3 Heat flux measurements for thermocouples' location....39
6.3.4 Mesh comparison....40
6.4 Study 1 conclusions....44
7 Study 2: single phase flow with nucleate boiling conditions....45
7.1 Case set up....45
7.1.1 Flow conditions....45
7.1.2 Expected results....46
7.1.3 Q applied to the heaters....46
7.2 Simulation results....46
7.2.1 Heat flux and temperature measurements for nucleation sites' location....47
7.2.2 Sensitivity analysis....48
7.3 Results comparison....51
7.4 Study 2 conclusions....51
8 Single phase conclusions....51
9 Modelisation of the experiment for the two phase simulation....52
9.1 Simulation simplifications....52
9.2 Mesh....52
9.3 Boundary conditions....53
10 Study 3: two phase flow....53
10.1 Case set up....53
10.1.1 Flow conditions....53
10.1.2 Expected results....54
10.2 Results and discussion....54

10.3 Study 3 conclusions 55
11 Environmental impact 56
12 Budget 56
13 Final conclusions and future steps 57
14 References 59

1. Introduction

It is a fact that our society's energy demand will become an issue in a few years. In this era, it is clear that the nuclear energy is an important factor in the daily energy production share.

Catalonia is a good example of this last statement, since more than half its energy consumption is obtained in nuclear power plants.

Therefore, given that the procedure needed in order to obtain electricity from nuclear power is complex and potentially dangerous, constant investigation and development in terms of security systems need to be done in order to use this energy in a safe way. This thesis is focused on the study of the boiling phenomena that might occur in the coolant of a nuclear reactor, which is crucial in terms of the distribution of the heat coming from the fuel rods. Boiling is, therefore, a notorious issue to take into account when thinking about nuclear fission reactor security. Furthermore, given that the majority of the reactors used in Sweden are Boiling Water Reactors, this study becomes even more important.

Today's technology allows us to improve study physical phenomena in several ways. Computers allow scientists and engineers to simulate experiments in order to get predictions of the results that will be obtained. In the same way, they also give the possibility to evaluate the results obtained in the real experimentation by comparing them to the simulation of equations or correlations.

The following results are the conclusion to the job done during a 6 month traineeship at the Nuclear Reactor Technology department of KTH, located in the Albanova Research Center, Stockholm.

1.1 Aim of the study and objectives

The main objective of this Master's Thesis is to simulate a real experimentation performed by Heiko Kromer[1] in the ABB Corporate Research center in Västerås, Sweden, which aimed to study the formation of sub-cooled nucleate boiling in a narrow water channel.

First, it is important to fully understand the physics that are involved in this study, such as the equations for the water transport, the heat transmission or the boiling events, among others. This will allow the author to assess the viability of the results obtained when simulating the model.

Then, it is crucial to evaluate the different tools and possibilities that are available, in order to simulate this experiment. Once this is decided, it is mandatory to fully understand its functioning, in order to be able to know the capabilities of the chosen tool.

The following step is to try to reproduce the model, as close as possible to reality. If simulating the whole phenomena is an unrealistic goal, then some approaches need to be done in order to obtain good results, while being aware of the limitations of the simulated model.

Finally, if some limitations are found in the simulations, some investigation needs to be done in order to express which further steps would the author have taken in order to improve his works.

1.2 State of the Art

In regards of empirical investigation to assess nucleate boiling parameters, there is a huge amount of bibliography published by numerous authors during the past years. Some examples of that are H.Anglart[2], Hibiki and Ishii[3] or Tomiyama[4], among many others that will be presented in this thesis. However, as it has been previously stated, many of those empirical correlations are only certain for specific experimental conditions, which is why there is the need to find new results that are less environmentally dependent.

There is a large background in the literature regarding both numerical and experimental studies related to the different boiling events, and more specifically to the sub-cooled boiling.

Due to the huge impact in nuclear reactor safety terms, numerical simulation of two phase flow using CFD has been implemented in many master's thesis and PhD's as main topic in KTH's Nuclear Reactor Technology department itself, not to talk about other institutions, where many other results can be found. Recent examples of this are A. Ghione[5] or E. Michta[6] Master's Thesis, written in 2012 and 2011 respectively.

As of the efforts made in the Nuclear Reactor Technology division at KTH, it has to be noted that several previous steps have been made in regards of the study of this topic. The first attempts were focused in studying a case where a cylindrical fluid channel was heated. That channel had high fluid velocities and turbulences. That experiment was simulated numerically, and a solver was created in order to solve it, which has been used in this thesis as well.

More recently, another experiment was done. In this case, the water channel was rectangular and narrow, and the fluid velocity was low, creating a laminar velocity profile. This is the experiment that is being simulated in this study.

2 Experimental set up

As it has been stated in section 1.1, Kromer's experimentation was an attempt to analyze the real behavior of boiling in the sub-cooled boiling regime. In order to do so, the experimental device consists of a water channel on top of an aluminium solid, which is heated by some cartridges in it. Thus, the water will increase its temperature up to the sub-cooled boiling regime. There is a set-up of high-speed cameras as well, in order to record the water flow and be able to obtain information about the bubble formation.

The research done in ABB by Heiko Kromer had the aim of determining sub-cooled nucleate boiling parameter values regarding bubble detachment frequency and diameter, to be further utilized in simulations. Despite the existence of empirical correlations regarding those parameters, new validations have to be performed in order to ensure its behavior in new experimental conditions.

The experimental device could be divided in three main parts, namely the water system, the solid or structural part, and the heating system. It also had secondary parts, such as the recording system, the polycarbonate layer and different insulations.

2.1 Water system

The water system included the water pumping system, the water channel and the accumulators. A representation of that system can be seen in Figure 1.

The rectangular water channel measured 3 mm deep x 100 mm wide x 401 mm height. This water channel acted as if it was the cooler in a nuclear reactor, extracting heat from the aluminium wall. The channel length was conceived to allow the flow to be hydrodynamically fully developed and, at the same time, to heat the water enough to create boiling conditions.

In order to get the water flowing through the channel, a pumping system was needed. According to Kromer[1], a low-flow pump (MICROPUMP, Model IEG 24V 9000rpm) was used for the experimentation.

The system also had to pre-heat the water up to a certain level, so it would be possible to attain boiling when the water went through the heated wall. In the real experiment, an accumulator (NÜVE NB 20, 15 Liters, 1600 W) was used in order to do so. Its function was to serve as reservoir of fluid and control the temperature in order to attain the desired conditions in the water channel inlet.

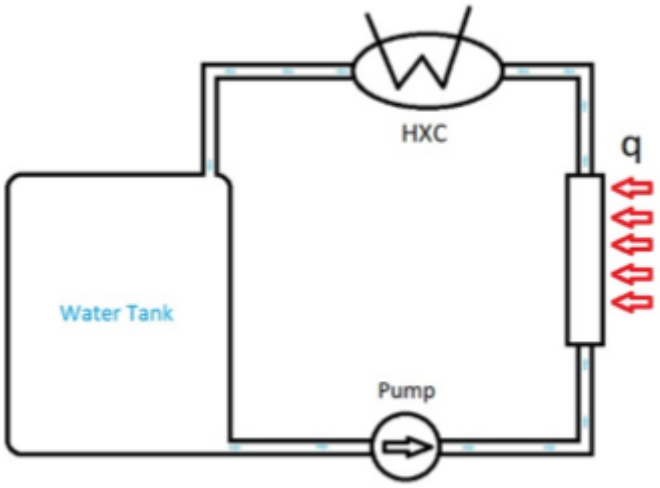

Figure 1 - Water sistem in the real experiment

2.2 Heaters

7 electrical heating cartridges were used in this experimental set up. They were cylindrically shaped, measuring 8mm radius and 80mm height. Being installed 22mm vertically separated from each other, the first one was installed at 175mm from the channel inlet in order to ensure that the water had time to fully develop a constant velocity profile. The distance between the heaters and the aluminium wall in contact with the water channel is 2mm.

The amount of heat produced by the heaters (Q_{out}) is controlled by the input voltage value they are given (U_{in}), according to Joule's law.

$$Q_{out} = \frac{{U_{in}}^2}{R} \tag{2.1}$$

Where R stands for the electrical resistance of the cartridge. Given that the resistance for each cartridge is 135Ω, it is fairly simple to control the amount of heat that comes out of them by manipulating the input voltage.

However, since the aim of this experiment was to produce boiling in the water channel, it was way more important to actually know which is the aluminium wall heat flux value (q'' $[\frac{W}{m^2}]$), coming as a result of the heat transfer from the cartridges to the aluminium block. The calculation of q'' is rough, since assessing heat losses is complicated in this case. Therefore, an insulation block was installed in the outer aluminium wall, just on top of the area where the heaters were located. The main goal of this insulation block was to try to decrease heat losses (which were estimated to be somewhere around 20%), so q'' could be obtained directly (or at least estimate it) by dividing the heat coming from the heaters by the heated area.

2.3 Aluminium block

The aluminium block was used as structural solid for the experiment. Its function is to heat the water in the channel as well, simulating the external Zirconium part of the fuel rods, which transfers the heat coming from the fission reactions in a real reactor.

2.4 Video recording system

In the real experimentation, a visualization system was created in order to obtain images of the bubble formation. It was mainly formed by high-speed cameras and a proper lightning system. The usage of high-speed cameras was explained due to the fact that when in the ONB, bubble formation, detachment and coalescence could barely take tenths of a second. Thus, there was the need to use high-speed cameras to successfully assess what was going on in the channel.

Figure 2 shows now the video recording system was implemented.

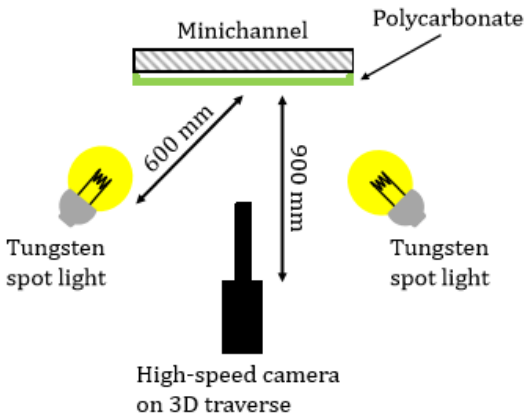

Figure 2 - Video recording system

2.5 Polycarbonate layer

A Polycarbonate (PC) layer was used in the experimentation, mainly in order to contain the water channel in the specified dimensions. Furthermore, there was the need to visualize the water flow during the experiment, so PC was the right material due to its transparency. The fact that PC has a low heat conductivity value provided heat containment in the water channel, which helped to enhance the boiling conditions in the water flow.

2.6 Insulation

The whole test body was insulated using UPM S2, an insulation material that was used in order to reduce heat losses to the achievable minimum. The insulation material has a thermal conductivity of approximately 0.35 W/m/K.

3 Phenomenology

In this section, the phenomenon that takes place in the experiment and its fundamental equations are described. The section is structured in (1) heating in single phase flow, (2) heating in the two phase flow and (3) solid region heating.

3.1 Single phase flow

First, the equations for single phase flow are presented.

Since the studied fluid is water, a Newtonian and incompressible fluid is assumed. In addition, the fluid variables are taken into account as constant.

The following equations are presented in mathematical notation. The corresponding discretized versions of those equations can be found in OpenFOAM's wiki[7] or in the files of the single phase solver itself, *chtMultiRegionFoam*[8].

3.1.1 Continuity equation

Given that the density is constant and that there is no input of fluid besides the inlet, the continuity equation is set as:

$$\nabla \cdot (U) = 0 \tag{3.1}$$

Where U stands for the fluid velocity. The term on the Left Hand Side of the equation (LHS) represents the divergence of the fluid velocity, or its variation in the control volume. Given that there cannot be variances in the fluid density, the continuity equation is simplified as it can be seen in eq. 3.1.

3.1.2 Momentum equation

The following equation solves the conservation of momentum.

$$\frac{\partial U}{\partial t} + \nabla \cdot (UU) - \nabla \cdot (\nu \nabla U) = -\nabla p \tag{3.2}$$

Where ν stands for the kinematic water viscosity.

In the first and second terms of the LHS, the temporal derivative of the fluid velocity and its advection are modelled. In the third one, the viscous stresses are taken into account. Finally, the term in the Right Hand Side (RHS) of the equation stands for the gradient of the pressure.

3.1.3 Energy equation

The equation below describes the conservation of energy in the fluid domain. Its terms are explained in this section.

$$\frac{\partial \rho h}{\partial t} + \nabla \cdot (\rho U h) + \frac{\partial \rho K}{\partial t} + \nabla \cdot (\rho U K) - \frac{\partial p}{\partial t} = -\nabla q + \nabla \cdot (\tau \cdot U) + pr + pg \cdot U \tag{3.3}$$

The first term in the LHS is the temporal derivative of the enthalpy (h). Describes how the internal enthalpy of the fluid varies for a period of time. The second term describes its advection, or how it varies in the volumetric dimensions.

The same happens with the kinetic energy of the fluid, represented in the equation as K, as the third and fourth terms of the LHS represent the temporal derivative and its advection as well.

The last term of the LHS of the equation describes the contribution of the pressure changes in the energy of the fluid.

The first term of the RHS is the heat flux vector, which indicates the volumetric derivative of the heat input. The second one is the term that represents the dissipation of energy due to viscous effects. The third term of the RHS is the heat source, which is zero in the cases where there is no heat generation in the control volumes that are being studied. And the last term of the RHS stands for the rate of change of potential energy, which is the one that is acquired due to the fluid gaining height.

Solving this equation will ensure the energy conservation of the fluid system.

3.2 Two-fluid model

As it has been done for the single phase flow, the two phase flow equations are presented. In fact, they are variations of the single phase ones, but taking into account that there are two phases in the fluid. Therefore, gas and fluid fractions are included, as well as some other terms.

Void fraction (α_a) stands for the fraction of volume of gas phase in the studied control volume. The same goes for (α_b), which is the fluid fraction. Given that this is a fluid that is divided in two phases:

$$\alpha_a + \alpha_b = 1 \tag{3.4}$$

New hypothesis are done for this fluid. Given that the vapor phase of water is compressible, the gas phase is taken into account as compressible and the liquid phase is incompressible. Both are Newtonian fluids.

The input variables of both fluids remain constant. The density of the void phase is calculated as:

$$\rho_a = P \cdot f \tag{3.5}$$

Where P is the pressure and f represents the compressibility factor of the gas, which is constant and equal to $5.90185 \cdot 10^{-6}$. It is considered that both fluids share the same pressure.

3.2.1 Continuity equation

First, the mass conservation equation is presented for each phase.

$$\frac{\partial(\alpha_k \rho_k)}{\partial t} + \nabla \cdot (\alpha_k \rho_k U) = \Gamma_k + \sigma \tag{3.6}$$

This equation describes conservation of mass, which is done due to the fact that the amount of mass of those phases increases or decreases because of boiling.

The first term of the LHS stands for the temporal variation of the phase mass, and the second one for the volumetric one. The first factor that can be seen in the RHS of the equation stands for the creation of phase, which is the effect of either evaporation of the liquid phase or condensation of the gas one. The second one is repeated from the equation for the single phase case, and is the source term.

3.2.2 Momentum equation

Following the same procedure, the momentum equation is presented. As in the previous case, the equation for one of the phases is presented.

$$\frac{\partial(\alpha_k \rho_k U_k)}{\partial t} + \nabla \cdot (\alpha_k \rho_k U_k U_k) = -\nabla p + \nabla \cdot (\alpha_k \nu \nabla U) + \alpha_k \rho_k g + \Gamma_{ki} U_i - \Gamma_{ki} U_k + M_{ki} \tag{3.7}$$

As in all the previous cases, the first two equations of the LHS represent the temporal and advective terms.

The first term of the RHS indicates the pressure variation. Note that this term does not depend on the phase, since they share the same pressure. As is happens in the single phase version of this equation, the second term of the RHS stands for the viscous stress and the third one for

the potential energy. The fourth and fifth terms appear in this version for the first time, and they add the velocity variation due to the change of the phase masses, due to evaporation and condensation of the fluid.

The last term stands for the interfacial momentum transfer term, i.e. the different forces that a bubble receives when it's surrounded by the liquid phase. The interfacial momentum transfer is a summation of the following terms.

$$M_{ki} = M^d + M^l + M^{wl} + M^{td} + M^{vm} \tag{3.8}$$

Which are respectively called the drag force, the lift force, the wall lubrication force, the turbulent dispersion force and the virtual mass force. Each one of those terms are explained in the sections below. It has to be noted that there exist many correlations to represent some of those terms. For brevity purposes, only the one that was used in the simulation is shown in the following sections.

3.2.2.1 Drag force

This force describes the resistance that exists when a bubble is moving through a fluid. It mainly depends on the bubble size and the relative velocity between the gas region (always noted as "a") and the fluid region (noted as "b") in which it is contained, $U_r = U_a - U_b$.

$$M^d = -\frac{3}{4}\frac{C_d}{D_s}\alpha_a \rho_b |U_r| U_r \tag{3.9}$$

Where D_s stands for Sauter Diameter, and is the diameter that the bubble acquires when it detaches from the wall.

There are many experimental correlations that can be used to calculate C_d. Schiller-Naumann[9], Ishii-Zuber[10], Wen-yu[11], and many more. However, as it has been stated before, only the first one will be presented.

According to the Schiller-Naumann correlation, C_d can be calculated as:

$$C_d = \max\left(\frac{24}{Re_b}\left(1 + 0.15 {Re_b}^{0.687}\right), 0.44\right) \tag{3.10}$$

Where $Re_b$is the bubble Reynolds Number, and is defined as:

$$Re_b = \frac{|U_a - U_b| D_s}{v_b} \tag{3.11}$$

This correlation is only valid for $Re_b < 1000$. Otherwise, C_d is considered constant and equal to 0.44.

3.2.2.2 Lift force

The lift force pushes the bubble towards the center of the pipeline or the wall, depending on its shape and size. It plays a significant role in the bubble distribution on the liquid phase, which is important to be taken into account when studying heat transfer on that region.

$$M^l = -C_l \alpha_a \rho_b (U_r) \times \nabla \times U_b \tag{3.12}$$

The Tomiyama[4] correlation is the one that is most taken into account to calculate this term. Therefore, it's the one that is going to be presented.

$$\begin{aligned} C_l &= \min(0.288 \tanh(0.121 Re_b), f(Eo_d)) && \text{if } Eo_d < 4 \\ C_l &= f(Eo_d) && \text{if } 4 < Eo_d < 10 \\ C_l &= -0.27 && \text{if } Eo_d > 10 \end{aligned} \tag{3.13}$$

$$f(Eo_d) = 0.00105 Eo_d^3 - 0.0159 Eo_d^2 - 0.0204 Eo_d + 0.474 \tag{3.14}$$

Where:

$$Eo_d = \frac{(\rho_b - \rho_a) g {d_h}^2}{\sigma} \tag{3.15}$$

$$d_h = D_s (1 + 0.163 Eo^{0.757})^{\frac{1}{3}} \tag{3.16}$$

$$Eo_d = \frac{(\rho_b - \rho_a) g {D_s}^2}{\sigma} \tag{3.17}$$

3.2.2.3 Wall lubrication force

The wall lubrication term represents the fact that it has been experimentally proven that the void fraction isn't usually concentrated touching the wall, but rather next to it.

$$M^{wl} = C_w \alpha_a \rho_b |U_r - (U_r \cdot n_w) n_w|^2 (-n_w) \tag{3.18}$$

Where n_w is the vector normal to the wall and U_r the relative velocity between the gas and liquid phases.

$$C_w = \frac{1}{2} C_{wl} D_S \left(\frac{1}{y_w^2} - \frac{1}{(D_{pipe} - y_w)^2} \right) \tag{3.18}$$

Where:

$$\begin{aligned} C_{wl} &= 0.47 && \text{if } Eo < 1 \\ C_{wl} &= e^{-0.933Eo+0.179} && \text{if } 1 < Eo < 5 \\ C_{wl} &= 0.00599Eo - 0.0187 && \text{if } 5 < Eo < 33 \\ C_{wl} &= 0.179 && \text{if } Eo > 33 \end{aligned} \tag{3.19}$$

And Eo is calculated as it was explained in section 3.2.2.3

3.2.2.4 Turbulent dispersion force

This term accounts for the way that the turbulent fluctuations on the fluid affect the gas bubbles. It's not interesting in the studied case in any means, since this case is laminar flow.

$$M^{td} = -\frac{3}{4} C_d \frac{\rho_b}{D_s} \frac{v_b^t}{\sigma_t} |U_r| \nabla \alpha_a \tag{3.20}$$

Where $\sigma_t = 0.9$ and C_d is calculated using the Schiller-Naumann[9] drag force coefficient correlation, which was presented in section 3.2.2.1

3.2.2.5 Virtual mass force

The virtual mass force stands for the force term added to the equation due to the effect of the accelerations that the fluid suffers when the bubble moves through it. This can be thought as an "extra" fluid phase mass. It is calculated in the following way.

$$M^{vm} = -C_{vm} \rho_b \alpha_a \left(\frac{DU_a}{Dt} - \frac{DU_b}{Dt} \right) \tag{3.21}$$

Where $C_{vm} = 0.5$ and $\frac{DU_x}{Dt}$ is the total derivative of the phase velocity.

3.2.3 Energy equation

This section includes the description of the energy balance equation for two phase flow. Please, note that this equation belongs to one of the phases, in this case, phase k. Therefore, another one needs to be implemented to describe phase i.

$$\frac{\partial(\alpha_k \rho_k h_k)}{\partial t} + \nabla \cdot (\alpha_k \rho_k U_k h_k) = -\nabla(\alpha_k q_k) + \frac{DP}{Dt} + \Gamma_{ki} h_i - \Gamma_{ik} h_k + \alpha_k q'' A_w \tag{3.22}$$

The first term of the LHS of the equation shows the temporal enthalpy variation for the phase k, and the second one shows its advection.

The first term of the RHS shows the direction of the heat flux in the specified volume. The second one stands for the total derivative of the pressure, where $\frac{DP}{Dt} = \frac{\partial P}{\partial t} + u \cdot \nabla P$. The third and fourth members of the RHS take into account the balance of energy due to evaporation and condensation. The last term represents the heat input from the heated wall to the water that is closest to the wall. It is described as the amount of heat flux times the wall area that the phase is in contact with.

3.3 Solid region

Heat transfer in solid region is modelled by a pure diffusion equation:

$$\frac{\partial \rho h}{\partial t} + \nabla \cdot \left(\frac{k}{Cp} \nabla h\right) = R \tag{3.23}$$

This balance takes into account the time and spatial derivative (advection) of the internal energy of the solid, which are the two terms on the LHS.

A separate term is used in the RHS to express the energy input, which in this case, occurs in the heaters. This term will be equal to zero when solving for the aluminium block.

3.4 Boiling phases

It is common knowledge that boiling is the effect that occurs to liquid phases when they are subjected to a certain amount of heat exposure, forcing them to change its phase to a gas state. Furthermore, boiling has a huge impact when the heated fluid is acting as a cold source in a heat exchanging system using forced convection, as in the case of nuclear reactors.

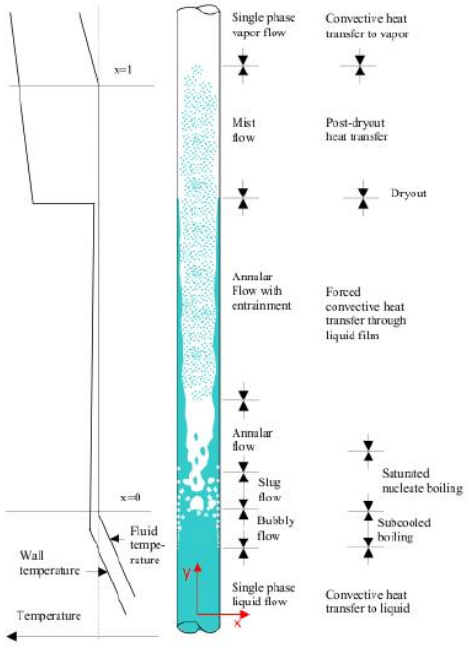

Figure 3 - Boiling phases related to wall and water temperatures

In a boiling process, the heat transfer coefficient varies substantially according to the phase, i.e. the type of boiling. Therefore, there are notable differences in terms of heat exchanging for the different boiling phases, being one of those called "subcooled nucleate boiling". The different boiling phases can be seen in Figure 4.

As stated in Anglart[2], boiling heat transfer can be represented in a logarithmic plot as a function between the wall heat flux (q'') and the wall superheat (ΔT_{sup}), which can be seen in Figure 4. Wall superheat stands for the difference between the temperature in the wall surface and the saturation temperature of the water adjacent to the surface.

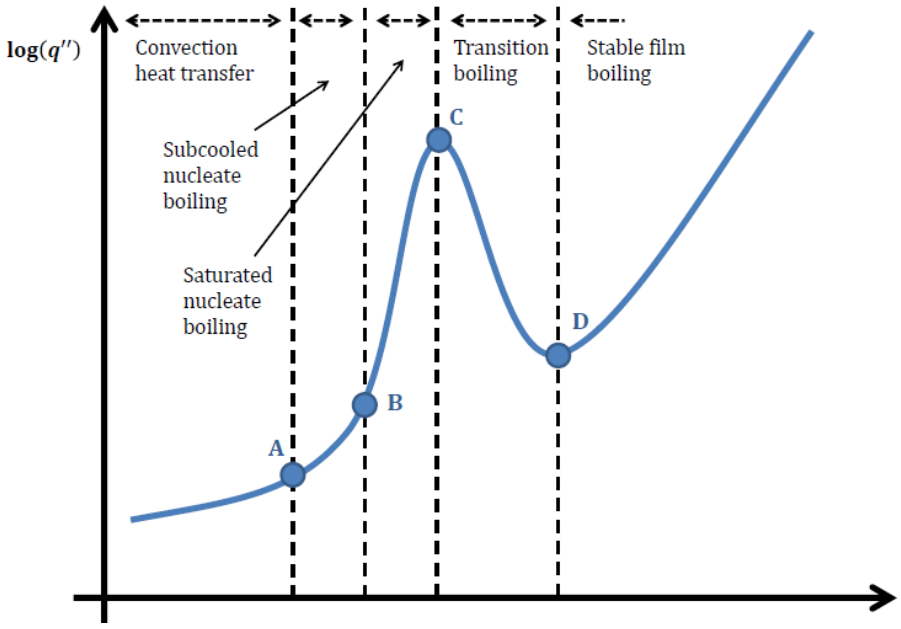

Figure 4 – Boiling phases

Up until reaching a certain wall superheat, the fluid is located in the onset of nucleate boiling (ONB) zone. There, the fluid can be conceived as single phase, and normal convection heat transfer terms can be utilized.

The subcooled nucleate boiling regime is contained within points A and B. Given the notable difference between the water temperature next to the wall and in the channel center, the phenomena known as “subcooled nucleate boiling” occurs. This means that bubbles are being generated in the water that is adjacent to the wall, but will condense when they detach from it and start migrating towards the channel center. This effect is really beneficial so as to enhance heat transfer rates, since a high wall heat transfer can be obtained while wall area occupied by gas phase is low enough to guarantee safe procedure.

The region compressed in between point B and C is called the saturated nucleate boiling regime. There, bubbles detach from the heated wall and do no longer condense in the channel center as the temperature differential isn’t high enough for that to happen.

The mark nominated as C shows the point where the critical heat flux (CHF) is reached. This means, as it can be seen in the previous plot that the wall heat flux will increase in a much more accused way from that point. This heat increase occurs due to the fact that the bubble generation rate has increased in such way that the majority of the wall area is now covered by vapor phase instead of liquid. Hence, the coolant is not able to extract heat as efficiently as it used to, since the convection heat transfer for vapor is much lower than for liquid phase water. This effect can be seen in Figure 3, in where one can see that the wall temperature increases drastically when the wall is in contact with the vapor phase.

If the Leidenforst point (marked in figure 1 as D) is reached, the bubble generation rate will have increased to the extent of creating a thin vapor phase film attached to the wall. This is the worst case scenario, in regards of unavailability of the refrigeration system to extract heat from the wall.

It has to be pointed out that this last situation is especially not desirable in nuclear reactors. As it can be seen in the previous figure, reaching the point where there is film boiling in the fuel rods would imply almost immediate temperature increases that could definitely damage them and thus develop into safety issues due to the unavailability to extract heat from the fuel rods. This situation could eventually imply the release of radioactive material to the primary system, which would clearly infringe the defense-in-depth safety and security principle.

4 CFD and OpenFOAM

4.1 Computational fluid dynamics (CFD).

In the cases where analytical solutions are not available, the two strategies to study fluid behavior are (1) experimental campaigns and (2) numerical simulation using Computational Fluid Dynamics (CFD) codes. Typically, both procedures are used, extracting data from the physical experimentation first, and then validating the obtained results with the CFD simulation in order to obtain a validated predictive tool, as it has been the case of this project.

CFD is a numerical methodology for solving equations, and requires 3 main steps, namely *pre-processing*, *solving* and *post-processing*.

- Pre-processing consists in generating a geometry, which is a simplified representation of a real device. Once the geometry is built, the mesh or grid must be defined according to the phenomenon to be studied and the available computational resources. In addition, physical assignments such as boundary conditions and material properties are included in the model as well.
- Solving means that the different equations that will be used for the case are discretized in space and time, and then solved for each cell of the mesh.
- Post-processing stands for using tools to visualize results once the solver has done its job.

Since complex CFD simulations are usually high demanding in terms of computational cost, the huge development of computers in the past years has had a huge impact in towards making CFD a reliable and powerful tool for engineering purposes.

Figure 5, which is extracted from the OpenFOAM user guide[12], summarizes what has been explained in this section.

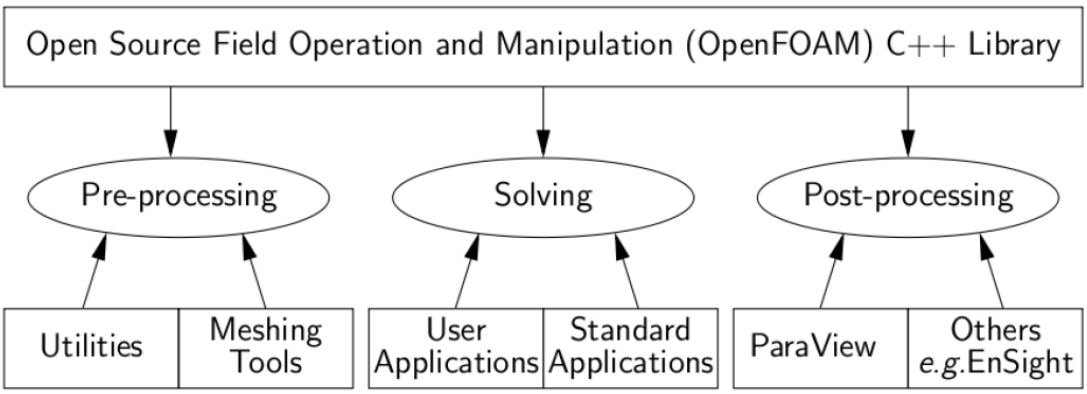

Figure 5 - Representation of OpenFOAM

4.2 OpenFOAM (Open Field Operation And Manipulation).

OpenFOAM ®, hereafter also known as OF, is an open-source framework created at the Imperial College in London in the late 1980's, releasing its first open source version in 2004. It is a very convenient tool for this project because of the following 3 reasons:

- It's *free of charge*.
- Its files are *open-source* i.e. the source code is available to everyone, and can be totally modifiable to what best suits the user.
- It is programmed as *object-oriented*, and uses C++ as the programming language. This means that the users can change parts of the code without having to modify the complete solver. For example, new features can be added in a solver so it suits the user's needs, or in the opposite case, some steps can be erased if they are not needed in order to reduce computational time.

In addition to what has been said until now, it has to be pointed out that another useful characteristic of OpenFOAM is how equations are managed in the code, since their representation is really close to the actual mathematical expression and thus, pleasantly user-friendly. An example of this can be seen in the OpenFOAM user guide[12], in section 3.1.3. The following equation:

$$\frac{\partial \rho U}{\partial t} + \nabla \cdot (\phi U) - \nabla \cdot (\mu \nabla U) = -\nabla p \tag{4.1}$$

Would be represented in OpenFOAM as:

```
solve
(
        fvm:ddt(rho, U)
      + fvm::div(phi, U)
      - laplacian(mu, U)
        ==
      - fvc::grad(p)
);
```

Which makes it easy for the user to handle equations.

4.3 Single phase solver: chtMultiregionFoam.

As it has been explained before, and according to OpenFOAM's description, *chtMultiRegionFoam* is a solver that calculates conjugate heat transfer between solid regions and fluid regions. In fact, it has been proven in this thesis that it can also handle heat transfer between two different solids.

The source code for *chtMultiRegionFoam* can be found in its source files[8]. The following section includes the key aspect of this solver.

4.3.1 Navier-Stokes algorithm (PIMPLE)

The solution is mainly performed by the PIMPLE loop, which is a combination of both PISO and SIMPLE loops. Given that PIMPLE is essentially a PISO loop with outer-corrector loops that allow it to obtain more precise solution, the PISO algorithm is the one that needs to be explained in depth.

The PISO concept (Pressure Implicit with Splitting of Operators) is one of the most efficient ways of solving the Navier-Stokes equations, which allows the solver to handle the velocity-pressure coupling. It treats the equations in an implicit way, which means that they take into account the values obtained in previous iterations. It calculates continuity errors and corrects flux and pressure values so as to obtain correct (and coupled) results for both velocity and pressure.

Given that the equations that are used for this algorithm are explained in section 3.1, they are not introduced again. The following lines describe the steps that the PISO algorithm takes to solve those equations.

1) Define the velocity equation in its discretized version.
2) Solve that equation, equaling it to the pressure gradient from the previous solution, making it implicit. The result obtained is the velocity prediction.
3) Obtain the mass fluxes from the velocity prediction.
4) Define the pressure equation using the velocity prediction and solved.
5) Correct the mass fluxes taking into account the pressure result.
6) Correct the velocity according to the obtained pressure field.

This algorithm will be repeated as many times as inner-corrector loops are set in the fvSolution file.

The PIMPLE loop adds the outer-corrector loops, which ensure the solution to have reached a certain amount of precision that is set by the user. Those loops check the residual for the solution. If that value turns out to be higher than the specified value, the solution will be calculated again through the whole PISO algorithm again.

4.4 Two phase solvers

In order to simulate the real experiment taking boiling into account, a solver that was able to calculate the equations explained in section 3.2 was needed.

In one hand, KTH's Nuclear Reactor Technology department already owned a solver that was able to calculate those equations. However, that solver was designed to solve a specific case that presented huge differences when compared to the one studied here. The solver was specifically designed for turbulent flow, which was believed to be a huge burden when trying to adapt that solver to our laminar case.

On the other hand, included in its version 3.0.0, OpenFOAM released a solver that is able to calculate phase change, named *reactingTwoPaseEulerFoam*[13]. It already takes into account both phases and the interaction between them, namely their evaporation and condensation. However, it lacks some things like the boiling parameters and the heat partitioning system, which means that it doesn't really solve boiling yet. By modifying and adding those equations to the solver, it is believed that the simulation could be solved. However, this possibility was not contemplated during the author's internship, and therefore will be taken into account as future steps.

5 Modelisation of the experiment for the single phase simulation

This section includes the different aspects regarding the creation of the model for the single phase flow simulation. It includes concepts such as the simplifications that were done to the model, the used measurements or pictures of the final model, among other concepts.

5.1 Simulation simplifications

There were parts in the real experiment that were designed to deliver the desired inlet conditions to the water flow. Given that this is obviously not needed in a CFD simulation, those systems were excluded from the simulated model. The same happened with all the parts that were designed to minimize heat losses in the real experiment. These conditions can be set by OpenFOAM without the need of simulating the material. Figure 6 shows the set-up of the real experiment.

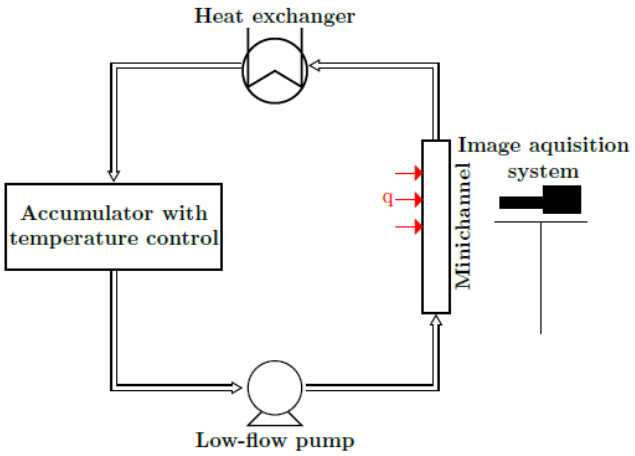

Figure 6 - Experimental system

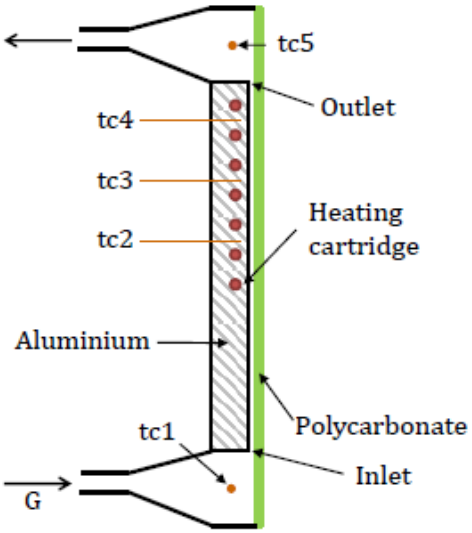

Figure 7 - Close-up of the experiment

Figure 7 shows the part of the experiment that was simulated in this study. The outlet temperature in the real experimentation was measured by the thermocouple tc5, in the outlet bath. The simulation allows the user to measure the temperature in the actual outlet, which is a few millimeters away from where tc5 was located in the real experiment. Therefore, the results delivered by the simulation should be equal or a bit higher than the experimental ones, given the energy losses that might occur from the outlet to tc5, but should be more representative of what is happening in the water channel.

The same happens with tc1. This value will not be measured in this case, but rather set in the inlet flow conditions.

Figure 8 shows the simulated experiment. It can be seen that many parts of the real experiment have been omitted, i.e. the pumping system, the inlet and outlet baths, the polycarbonate layer, and the image acquisition system.

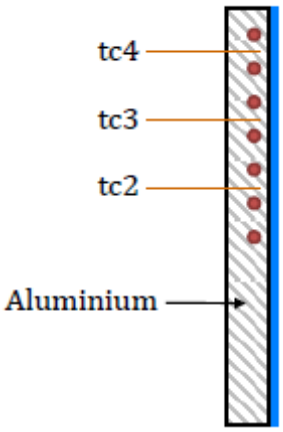

Figure 8 - Simplification used in the simulation

5.2 Geometry and dimensions

The measures that were used to create the model have been extracted from both Al-Maeeni's[14] Master's Thesis and Kromer's[1] report. Figure 9 shows the exact measurements of the real device, which were implemented in the simulated model. It has to be taken into account that, as it has been explained before, the model has been simplified, meaning that some parts have been erased due to them being unnecessary for the model.

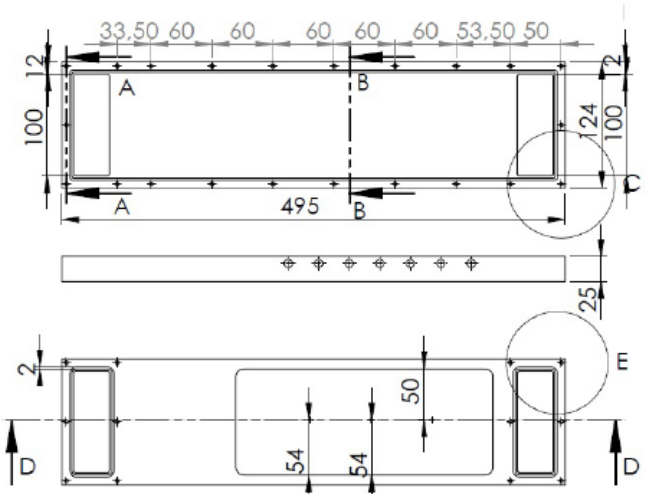

Figure 9 – Real device measurements

Figure 10 shows the simulated model for the water channel

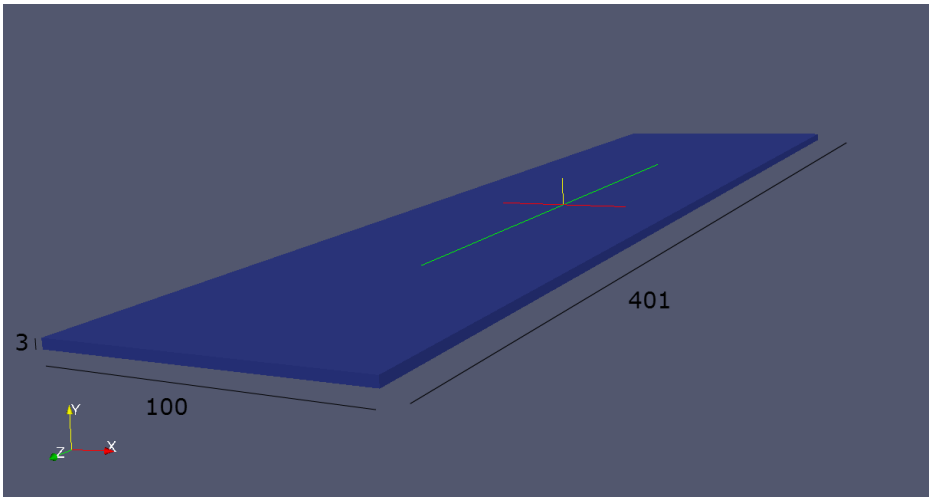

Figure 10 – Simulated water channel, with axis

Figures 11, 12 and 13 show different regions of the model. Playing with the opacities of the different bodies, all the parts are assembled for the easier understanding in regards of the model design and the localization of the regions.

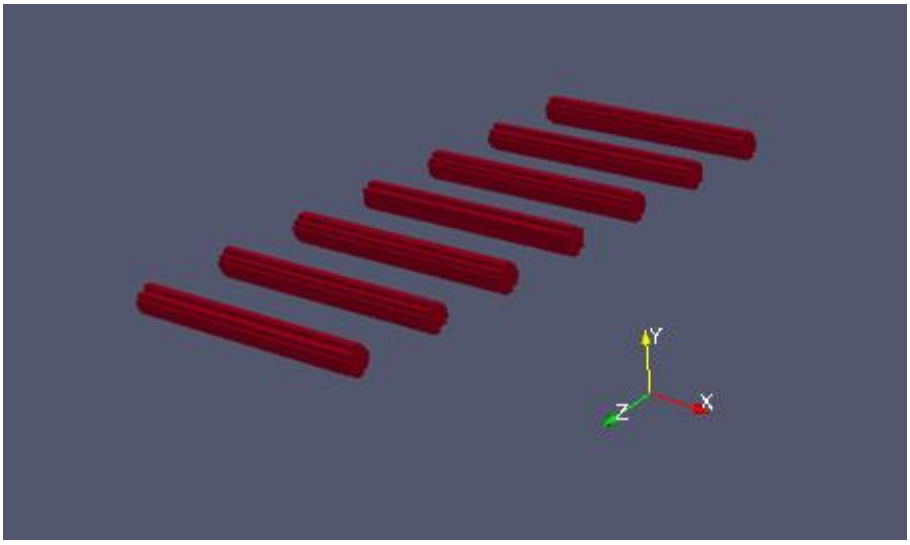

Figure 11 - The simulated heaters

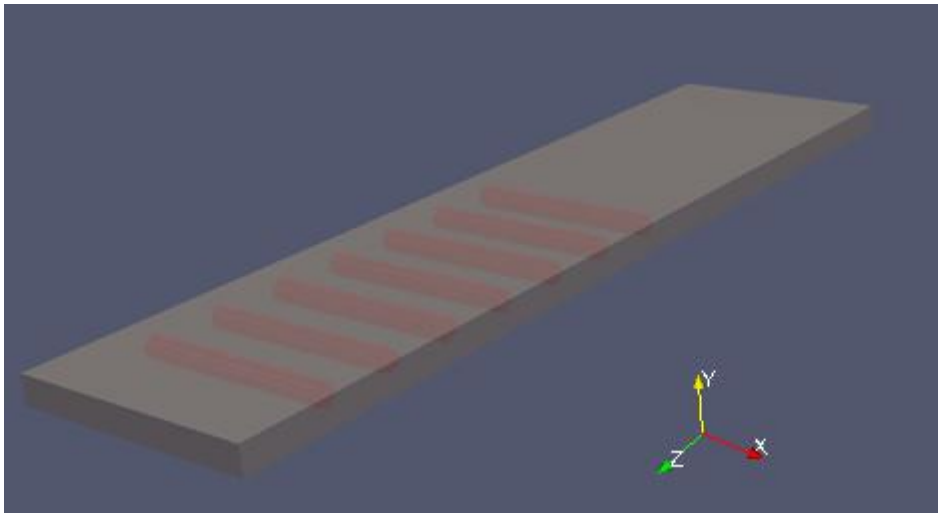

Figure 12 - The simulated heaters inside the aluminium block

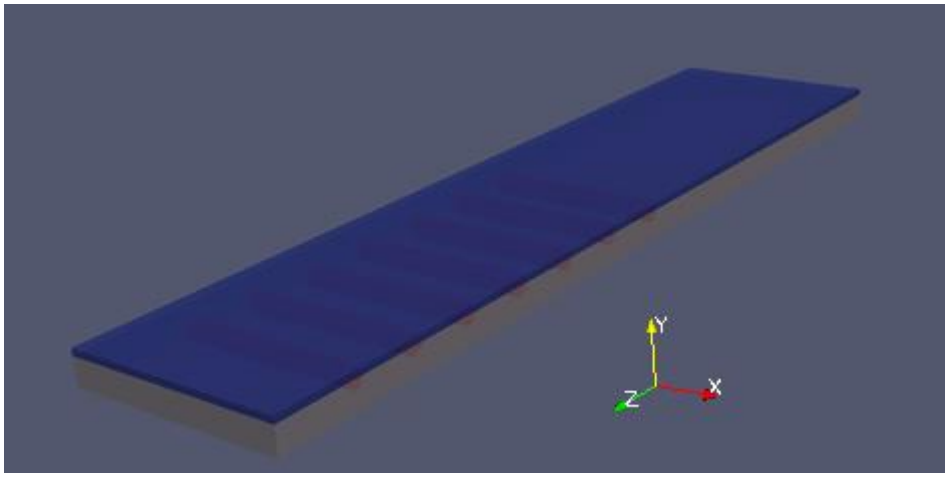

Figure 13 - The whole simulated model

5.2.1 Axis definition

The following sections will make reference to the different axis that were set in the model, namely the X, Y and Z axis. Even though these axis can be seen in all the figures of the section above, this is done in order to clarify the direction of those vectors.

The Z axis is the direction in which the water flows. Its vector is normal to the water inlet.

The Y axis is the one that represents the depth of the water channel and the aluminium block. Its vector is normal to the heated aluminium wall.

The X axis can be represented with the width of the water channel. It is the axis of the longitudinal vectors of the heaters.

5.3 Mesh

This section presents the mesh that was used in studies 1 and 2.

The mesh consists in two blocks of tetrahedral cells, namely the aluminium block and the water block. They are respectively represented in red and blue in Figure 14. The aluminium block consists in 30 cells in the X direction, 8 cells in the Y direction and 500 in the Z direction.

The water block is a bit different, since the number of cells in the Y direction has been increased to 10 cells and a cell height gradient has been used. This last concept means that the last water cell is 10 times bigger than the first one. This has been used in order to refine the mesh (i.e. include more cells) in the water zone that is closer to the aluminium wall, where the data is going to be extracted from.

The heaters region is not included in this part, since it is mainly a region of the aluminium block where the heat has been set.

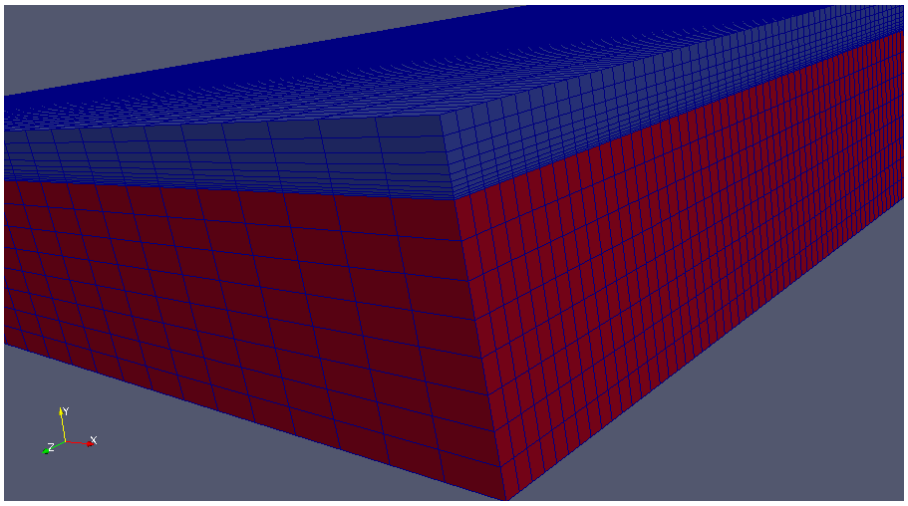

Figure 14 - Mesh close-up

5.4 Boundary conditions and numerical strategies

In this case, since the external walls of the solid are adiabatic, they were set to not change their temperature, using the *zeroGradient* (BC) provided by OpenFOAM. For the external walls of the model that are in contact with water, the non-slip condition for the flow velocity was set, which means that the water in contact with the specified wall has its velocity nullified.

In addition, the heat needs to flow from the heaters to the aluminium block, and from there to the water channel. In order to achieve that, a BC that imposes the same temperature value for both sides of a patch was used (eq. 5.2). It also means that the heat flux is conserved when transmitted from one region to the other (eq. 5.1). The BC used in this case is "*turbulentTemperatureCoupledBaffleMixed"*, and applies the following equations.

$$(k\nabla T)_{R1} = (k\nabla T)_{R2} \tag{5.1}$$

$$T_{R1} = T_{R2} \tag{5.2}$$

Where k stands for the thermal conductivity of the respective material, and R1 and R2 are the different regions for which the BC is set.

In regards of the inlet, a uniform velocity is set. It is expected for the model to create a fully-developed laminar velocity profile though the length of the channel, which is why the velocity wasn't set as a profile. The inlet temperature is set as well.

Finally, the fully developed flow conditions are set in the outlet, by imposing the zero gradient BC for the velocity.

In regards of the used time step (Δt), the Courant number has been respected, meaning that the time step is calculated for each iteration according to the following equation.

$$C = \frac{u\Delta t}{\Delta x} \leq 0.2 \tag{5.3}$$

Where u is the magnitude of the fluid velocity and Δx is the magnitude of the length of the model.

As of the numerical schemes, the first order temporal scheme was used. For the spatial discretization, the upwind variant was used for the advection term, and the central difference for the other terms.

5.5 Post-processing procedures

The following procedures/utilities have been used to obtain the desired results from the simulations.

5.5.1 Heat through the wall

The amount of heat that is through the walls of the aluminium solid is assessed in this section. It has two purposes, i.e. to ensure that the BC that provides adiabaticity to the model is working properly, and to assess the amount of heat that is being transmitted through the hot wall towards the water channel. This is calculated with the following equation.

$$q = \int k \nabla T \, dA \tag{5.4}$$

Where k is the thermal conductivity of the aluminium, T is the temperature and A is the area of the hot wall.

OpenFOAM offers a utility that calculates the discretized version of the equation above for a given patch. It's called *wallHeatFlux.*

$$q = \frac{\sum_i k \left(\overrightarrow{\nabla_{sn}} T \cdot \left|\overrightarrow{S_f}\right|\right)}{\sum_i \left|\overrightarrow{S_f}\right|} \tag{5.5}$$

Where $\left|\overrightarrow{S_f}\right|$ is the surface vector that is normal to each cell, and ∇_{sn} is the surface normal gradient, in this case of the temperature.

5.5.2 Average outlet temperature

This utility will be used to match the experimental outlet temperature with the one obtained in the simulation.

In order to obtain the average temperature at the outlet, the following formula has to be used:

$$T_{exit\ exp} = \frac{1}{A} \int T \, dA \tag{5.6}$$

Where A stands for the calculated area, and T for the temperature.

OpenFOAM offers a utility that solves the discretized version of this equation for a given patch, which is called *patchAverage*. The equation that is solved by this utility is the one that follows.

$$T_{exit} = \frac{\sum_i T \left|\overrightarrow{S_f}\right|}{\sum_i \left|\overrightarrow{S_f}\right|} \tag{5.7}$$

Where $\left|\overrightarrow{S_f}\right|$ stands for the surface vector that is normal to the calculated faces.

As it can be seen, the discretized version of the equation essentially consists in multiplying each cell value for the cell's area, adding them all up and then dividing by the area of the patch.

Hence, using this utility at the outlet patch of the water channel will provide the weighted average temperature in the channel outlet.

5.5.3 Wall temperature values for thermocouple positions

The following figure shows the position of the thermocouples used in the real experiment, which were implemented in the simulation. According to the coordinates used in the simulation, the thermocouples have been located at 221 (tc2), 281 (tc3) and 336 (tc4) mm (z axis) from the inlet, and in the middle of the channel. Figure 15 describes the position of these thermocouples.

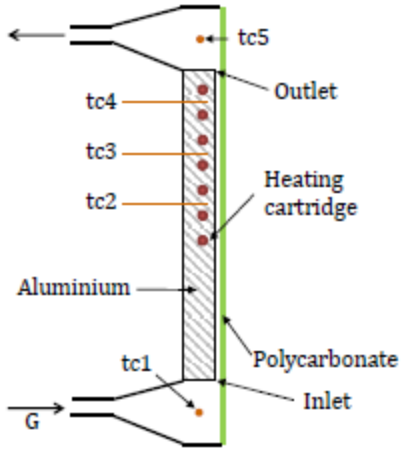

Figure 15 - Position of the thermocouples

Hence, the sampling method has been used to acquire wall temperatures for those positions in the simulation. These values will be later compared to the experimental results in order to extract conclusions.

5.5.4 Cell and wall values for nucleation sites

Once the outlet temperature has been proven to be correct, it is time to process data for nucleation sites. T_w, U_{f1}, U_{f2}, T_{f1} and T_{f2} have been directly obtained by sampling data from the simulations. Its locations can be seen in figure 11. q'' has been manually calculated from the temperature gradient between the wall and the first cell of the respective regions.

Figure 16 shows the coordinate system that was used to label the nucleation sites in the real experiment.

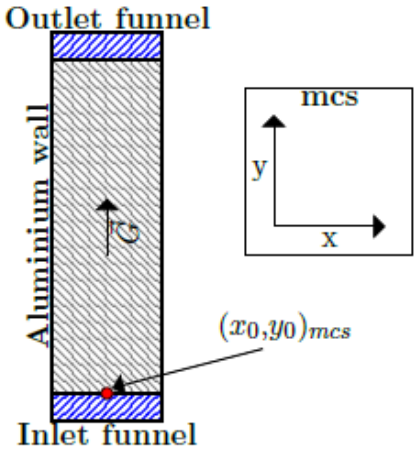

Figure 16 - Coordinates used by Kromer to idenfity Nucleation Sites

It has to be reminded that this simulation does not include the inlet and outlet funnels. Hence, the aluminium block actually is the grey part that is seen in the figure above. In addition, *y* in Kromer's reference system is named *Z* in the one used in the simulation. Therefore, y_0 in Kromer's location system is the same position as Z=0 in this study's mesh.

Figure 17, which is shown below, describes the location in where the nucleation sites appeared in the real experimentation.

Nucleation site label	Real position x in mm	Real position y in mm	Identified position x in mm	Identified position y in mm	Accuracy mm
1	2.1	210.0	2.4	210.2	0.4
2	5.5	207.8	5.5	207.9	0.1
3	13.0	206.8	13.0	207.1	0.3
4	4.7	203.7	4.8	203.8	0.1
5	2.6	203.0	2.6	203.1	0.1
6	9.9	200.3	10.0	200.7	0.4
7	3.7	200.1	3.8	200.2	0.1
8	-0.1	199.3	0.0	199.7	0.4
9	10.0	213.5	10.1	213.4	0.1
10	15.9	213.2	15.6	213.0	0.4
11	-[a]	-[a]	-3.4	212.4	-[a]
12	-[a]	-[a]	16.2	207.0	-[a]
13	15.9	201.4	15.3	201.6	0.6
14	16.4	198.8	15.6	199.2	0.9
15	-3.7	199.6	-4.2	198.7	1.0

Figure 17 - Localization of the Nucleation Sites

The sampling utility was used to obtain data for each nucleation site. Figure 18 shows the location in each cell center in where the previously described values were gathered, for each nucleation site.

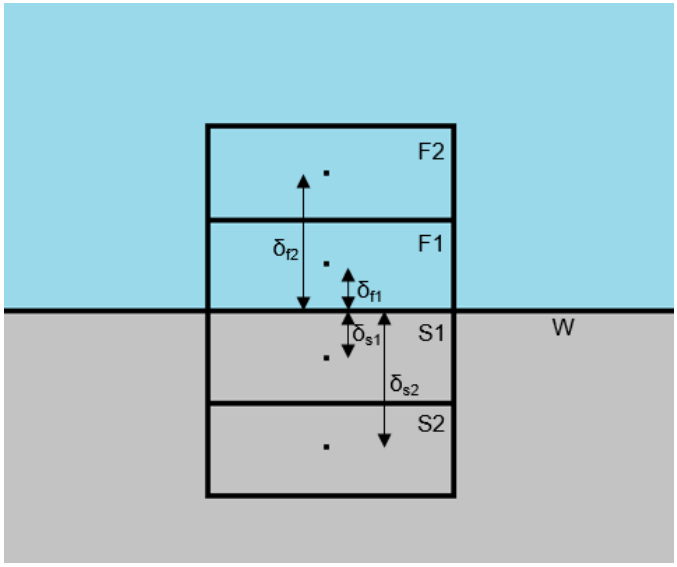

Figure 18 – Sampling locations in each nucleation site

The schematic shown in Figure 18 shows where the sampling system acquired data. For each nucleation site, temperature and velocity measurements in the center of the two closest cells to the wall (for both fluid and solid regions) were made.

Once the respective velocity and temperature values for each cell have been acquired, q'' is calculated using the following formula:

$$q'' = \frac{T_{wall} - T_{s1}}{\delta_{s1}} \cdot \lambda_{Al} = \frac{T_{wall} - T_{f1}}{\delta_{f1}} \cdot \lambda_{H_2O} \tag{5.8}$$

5.5.5 Sampling setup

A script has been written for the sampling system, as well as specific documents for the sample dictionaries that will be explained in this section.

5.5.5.1 nucleationSites

In order to facilitate the gathering of information for other locations, the sampling locations have been externalized in a document that can be found in the case folder, named *nucleationSites*. This makes it possible to change the locations only in this file, instead of having to change it in all the different *sampleDicts*.

nucleationSites

```
// Nucleation sites

ywall       0.023;
ys1      0.0217;
ys2      0.0212;
yf1      0.02306;
yf2      0.02308;

xns1        0.0521;
xns2        0.0555;
xns3        0.063;
xns4        0.0547;
xns5        0.0526;
xns6        0.0599;
xns7        0.0537;
xns8        0.0499;
xns9        0.06;
xns10       0.0659;
xns13       0.0659;
xns14       0.0664;
xns15       0.0463;

zns1        0.21;
zns2        0.2078;
zns3        0.2068;
zns4        0.2037;
zns5        0.203;
```

Figure 19 - nucleationSites document

Figure 19 shows an example for the *nucleationSites* file. The "y" values that can be seen in the first lines specify the location of the wall and the first two solid and fluid cells closer to the wall. Those values depend on the mesh that has been used, so they only need to be changed if the mesh is.

xns and *zns* refer to "x position nucleation site" and "z position nucleation site". Nucleation sites are located in a certain *x* and *z* position, and then data is sampled for all the y values.

It is important to take into account that there's a difference between the coordinate system used by Kromer and the one used in this simulation. Due to the fact that Kromer located x=0 in the center of the aluminium block and the simulation locates it in one of the corners, all the *x* values that he described need to have 50mm added (half of the width of the aluminium block) to them in order to actually refer to the same location.

For example, it can be seen in table 1 (Section 3.4) that Kromer describes the first nucleation site as x = 2.1mm and y = 210mm. In the nucleationSites file, this would be translated as xns1 = 0.0521 (2.1 mm + 50 mm converted to meters) and zns1 = 0.21.

5.5.5.2 sampleScript

This is the script that has been created to obtain data for the nucleation sites. The script will sample the locations that have been specified in the *nucleationSites* document, and will summarize all the data in a document called *allInfo*, which will be found in the *postProcessing/allInfo* folder once the script has been run. This can be done by typing *./sampleScript* in the command prompt once the case has been solved.

allInfo

```
Tc1_T.xy
0.05    0.023   0.221   392.1584
Tc2_T.xy
0.05    0.023   0.281   398.94172
Tc3_T.xy
0.05    0.023   0.336   400.65723
fluid1_T.xy
0.0521  0.02306     0.21    389.64147
0.0555  0.02306     0.2078  389.47096
0.063   0.02306     0.2068  389.15804
0.0547  0.02306     0.2037  388.64212
0.0526  0.02306     0.203   388.66608
0.0599  0.02306     0.2003  387.70026
0.0537  0.02306     0.2001  387.7475
0.0499  0.02306     0.1993  387.53954
0.06    0.02306     0.2135  389.89983
0.0659  0.02306     0.2132  389.65315
0.0659  0.02306     0.2014  387.99152
0.0664  0.02306     0.1988  387.07502
0.0463  0.02306     0.1996  387.51614
fluid1_U.xy
0.0521  0.02306     0.21    -1.9657172e-08  1.9766805e-09   0.0042208732
0.0555  0.02306     0.2078  -3.9790109e-07  2.124302e-09    0.0042210909
0.063   0.02306     0.2068  -8.2218758e-07  2.257357e-09    0.0042214138
0.0547  0.02306     0.2037  -4.0882132e-07  2.3720102e-09   0.0042217869
0.0526  0.02306     0.203   -2.0962813e-08  2.3150373e-09   0.0042217789
0.0599  0.02306     0.2003  -4.5823928e-07  2.4182943e-09   0.0042223896
```

Figure 20 - allInfo document

Figure 20 shows an example of how *allInfo* summarizes all the obtained data. The first 3 values of each line show the x, y and z position in where the sampling has been made, and then the result is shown.

6 Study 1: single phase flow

Single phase flow was used for this study, since the main objective for the first steps was to develop a case that was able to simulate the model and sample data in the nucleation sites that were specified in Figure 17.

Given that single phase flow is being studied, boiling was not taken into account during this part of the project, nor the effects that boiling implies in the heat transfer of the studied fluid.

For this study, the fluid is considered Newtonian and uncompressible. In addition, its thermophysical properties are set as constant.

In order to achieve this, the chtMultiRegion solver described in section 4.3 has been used.

6.1 Case set up

This section includes the different set up concepts that are part of Study 1. The hypothesis used are the ones that have been indicated in section 3.1

6.1.1 Flow conditions

The following list includes the most characteristic variables that were set for this simulation.

$T_{in} = 90ºC$

$\mathrm{G} = 134.2\ \frac{kg}{m^2 s}$

$\mathrm{q}'' = 5\ \frac{W}{cm^2}$

$p = 1\ atm$

$\rho_{l\ inlet} = 965 \frac{kg}{m^3}\ (1\ atm, 90ºC).$

$A_{channel} = 3x100mm^2 = 0.0003m^2$

$$U_{in} = \frac{G}{\rho_{l\ inlet}} = \frac{134.2\ \frac{kg}{m^2 s}}{962\ \frac{kg}{m^3}} = 0.1395 \frac{m}{s}$$

$$\overline{C_p} = \frac{h_{out} - h_{in}}{T_{out} - T_{in}} = \frac{406450 - 376990}{97 - 90} = 4208.57\ \frac{J}{kg \cdot K}$$

$\mu_{in} = 0.3144\ x\ 10^{-3}\ Pa \cdot s$

6.1.2 Expected results

The experimental measurements for this study can be found in the following figure. Temperature values of the previously studied thermocouples are shown. As it has been previously stated, the objective of this simulation is to compare the obtained results with these ones.

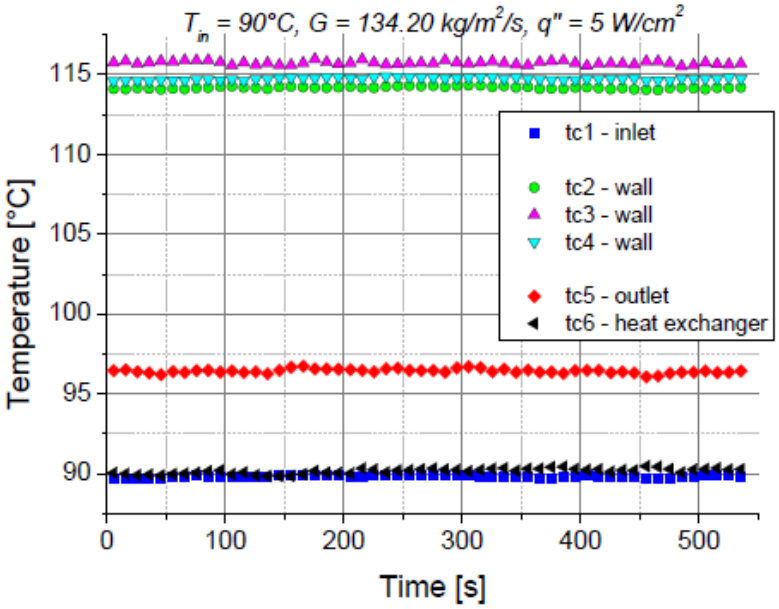

Figure 21 - Experimental results for the first study

It can be seen in Figure 21 that the expected results are respectively:

$T_{out} \cong 97.5ºC$
$T_{thermocouples} \cong 115º$

The post-processing procedures explained in section 5.5 will be used to compare the simulation and the experimental results.

6.1.3 Q applied to the heaters

The heated area that was mentioned in Kromer's report was used in order to calculate the amount of heat that should be applied in the heaters, taking into account that the model has no heat losses.

$$Q_{heaters} = q'' \cdot A_{heated} = 5\ \frac{W}{cm^2} \cdot 203.2\ cm^2 = 1016\ W \tag{6.1}$$

6.2 Simulation results

The following section presents the results that were obtained in the simulation for this study.

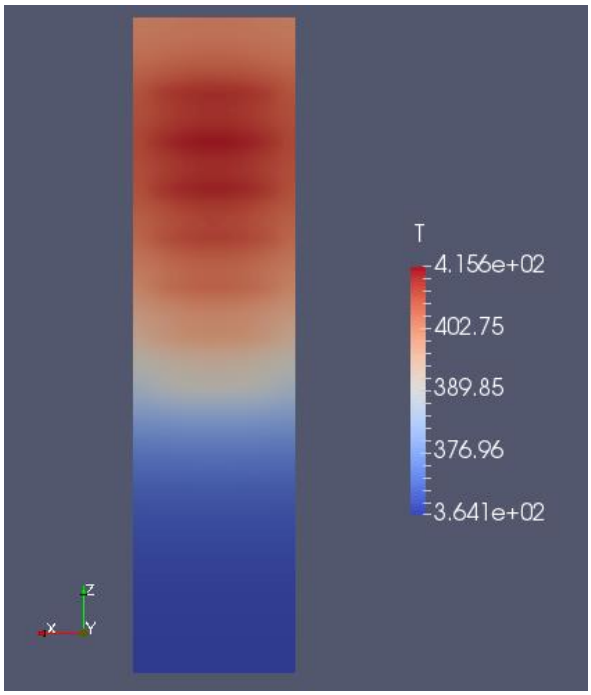

Figure 22 - Aluminium block temperature distribution, Study 1. Temperature in K

Figure 22 shows the temperature distribution of the aluminium block. It can be seen that the highest temperature values appear in the location of the heaters, making it possible to see their location.

In addition, it can be seen how the temperature affects the water when it has already traveled some distance in the channel. This is beneficial, since it allows the flow to develop its velocity profile before being affected by the heat input.

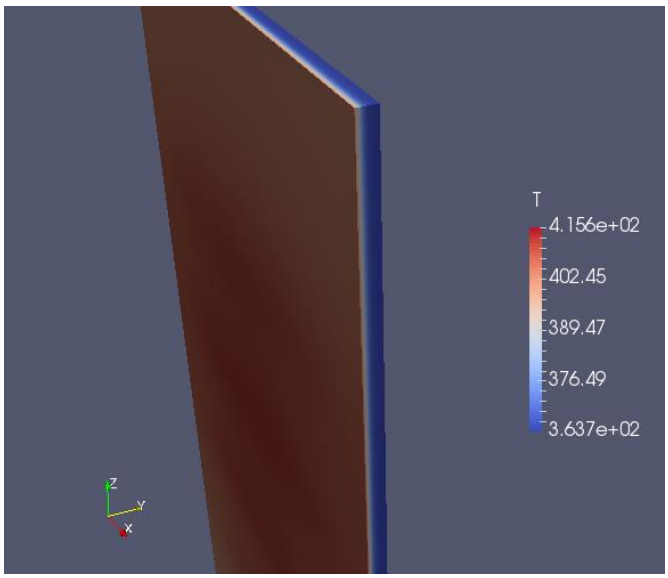

Figure 23 - Water temperature profile at the channel outlet, Study 1. Temperature in K

Figure 23 shows how the water temperature profile is being developed in the channel, showing the channel outlet. The hottest water temperatures are achieved in the part of the channel that is in contact with the heated aluminium wall. It can be seen that this channel allows the formation of sub-nucleate boiling, since there are big temperature differences between the different depth levels of the channel, even though is the channel is narrow. The water temperature in the hottest part allows boiling, while the other part of the channel is way colder, meaning that the bubbles will condensate there.

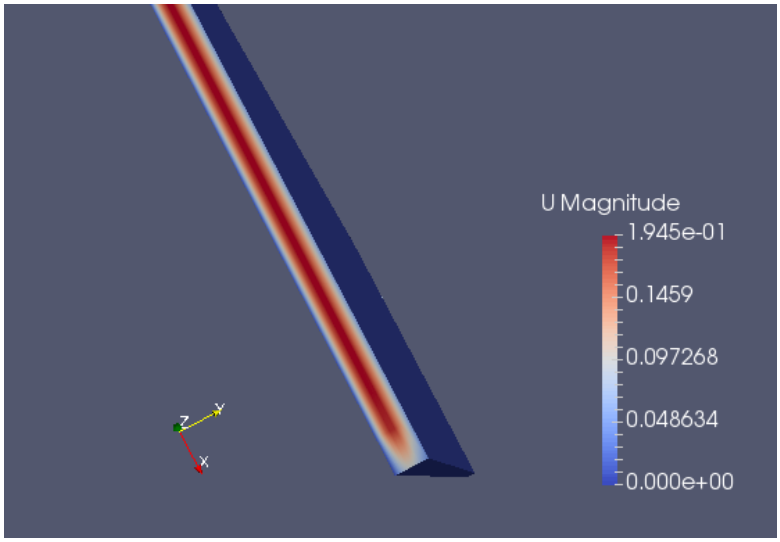

Figure 24 - Water temperature profile in the outlet, Study 1. Velocity in m/s

Figure 24 shows the water profile in the outlet. It proves that the previously set boundary conditions are working properly, since the water velocity in the different channel boundaries is set to 0. It can be seen that the maximum water velocity is obtained in a certain distance from the channel walls, which confirms that there is a water velocity profile.

Given all these results, it can be seen that the model is behaving properly. Therefore, the results are taken into account as correct and the following sections will compare the obtained measurements with the experimental ones.

6.3 Results comparison

This section compares the values obtained in the simulation to the expected results, which were shown in section 6.1.2.

6.3.1 Outlet water temperature and heat assessment

The first result to be compared is the average temperature in the outlet. Using the procedure described in section 5.5.2, the obtained average outlet temperature value in the simulation is 371.656K (98.5ºC). Given that the experimental results were measured in the outlet bath, which was omitted in the simulation, it is clear that the obtained result should be equal or slightly higher than the one measured in the real experiment. The expected result was ≈ 97.5ºC, so it is concluded that the simulated output temperature is correct.

Then, the heat transfer through the hot aluminium wall is measured using the concepts explained in section 5.5.1. This is done in order to assess if the BC that should ensure adiabaticity in the model are working properly, and to ensure that all the heat that is produced in the heaters is indeed being transferred to the water.

When using the procedures described in section x, the results show that the integrity of the heat is transferred from the heaters to the aluminium block, and that 998.46W are going through the aluminium wall to the water. Given that the amount of heat that was set in the heaters is 1016W, the amount of error is 1.7%. Since OpenFOAM uses the discretized version of the equation presented in section 5.5.1, it is clear that some errors might occur when it is applied to big areas. Therefore, the obtained error is considered to appear due to numerical errors and thus is neglected.

6.3.2 Wall temperature discussion

Figure 25 shows the wall temperature on the Z axis for the simulation, and can be compared with the experimental results.

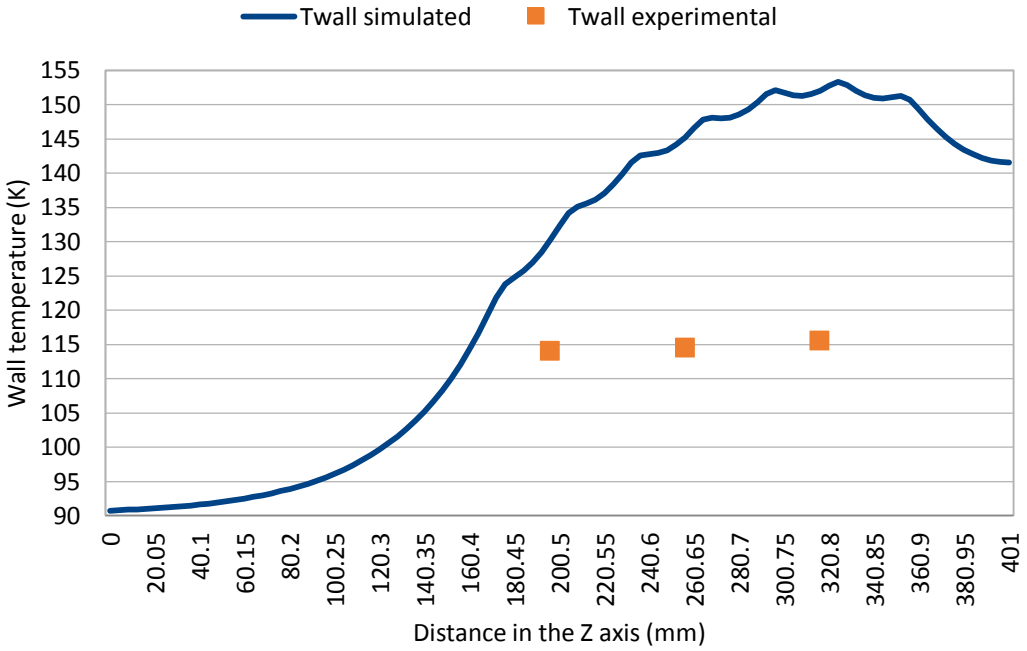

Figure 25 - Wall temperature comparison

It can be seen that the simulated temperature is nowhere close to the experimental values. That happens due to the fact that single phase flow is being studied. This topic is explained in further sections.

6.3.3 Heat flux measurements for thermocouples' location

Following the post-processing procedures explained in section 5.5.4, the heat flux q'' is measured for each thermocouple. The results obtained are summed up in the Table 1.

Position	Variable name	Experimental data	Simulation
Thermocouple 1	Tc1 [ºC]	≈114,5	127,98278
(221 mm from inlet)	Ts1 c1 [ºC]	-	128,29948
	q''_{wall} c1 [W/cm^2]	-	2,57966
Thermocouple 2	Tc2 [ºC]	≈115	137,14429
(281 mm from inlet)	Ts1 c2 [ºC]	-	137,29948
	q''_{wall} c2 [W/cm^2]	-	2,566603
Thermocouple 3	Tc3 [ºC]	≈116	139,48837
(336 mm from inlet)	Ts1 c3 [ºC]	-	139,61508
	q''_{wall} c3 [W/cm^2]	-	2,095588462
Outlet	Toutlet [ºC]	≈97,5	98,50681

Table 1 - Temperature and q'' for Thermocouples, Study 1

6.3.4 Mesh comparison

To be able to see if there is mesh dependency on the obtained results, a mesh refinement assessment has been done. Four types of meshes were used in this study, and plots for the most interesting variables were done in order to compare results.

The first case has been used for this study, with a diminishment of the 20% on the heat input value, which simulates heat losses in the aluminium block. This was done to try to lower the obtained wall temperatures to obtain physically understandable values, allowing to study the mesh in a case that is closer to reality.

The simulation was done once until it showed proof to be in steady state, meaning that the results were not changing even if the simulation was run for more time. In this study, the time to obtain a safe steady state was 200 seconds.

6.3.4.1 Used meshes and computational time

Mesh 0:

61.600 cells.

Execution time for 200s simulation = 1507s -> 00:25:07 (HH:MM:SS)

Mesh 1:

162.000 cells.

Execution time for 200s simulation = 6047s -> 01:40:47 (HH:MM:SS)

Mesh 2:

270.000 cells.

Execution time for 200s simulation = 16847s -> 04:40:47 (HH:MM:SS)

Mesh 3:

500.000 cells.

Execution time for 200s simulation = 24803s -> 06:53:23 (HH:MM:SS)

The following graph plots the relation of the number of cells and the time that the solver needs to calculate 200s of simulation.

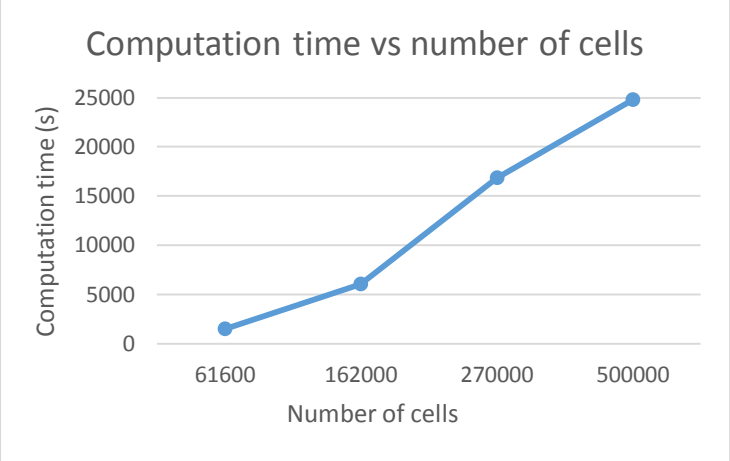

Figure 26 – Computation time vs number of cells

Figure 26 shows that there is a linear correlation between the number of cells and the computation time, as it should be.

6.3.4.2 Graphs through the Z axis

The upcoming graphs were done following the line that is presented in Figure 27. The line is set for it to touch the aluminium wall, from inlet to outlet. Wall temperature will be measured in this graph.

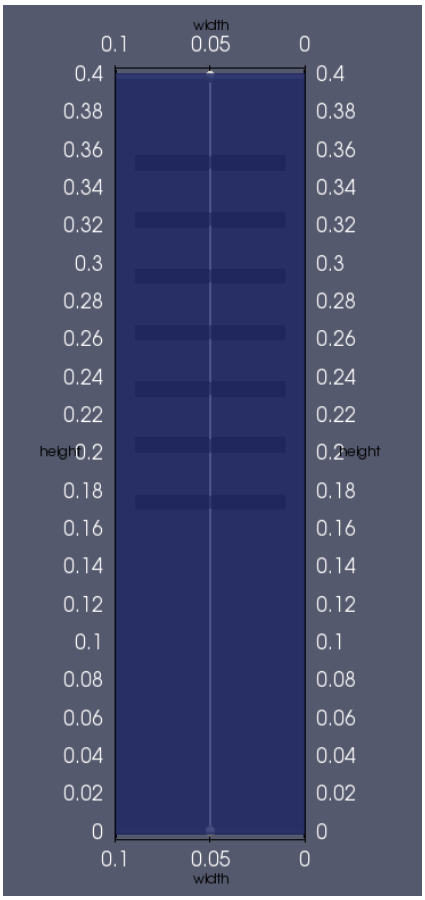

Figure 27 - Z axis plot line

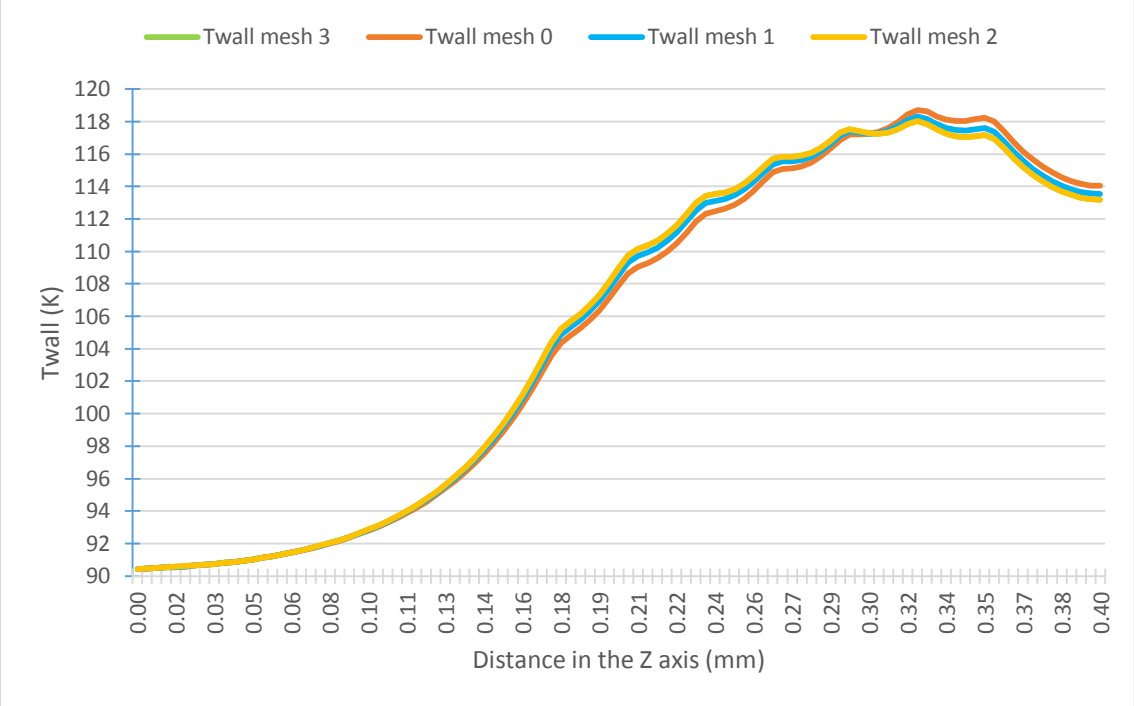

Figure 28 - Z axis wall temperatures

It can be seen from the comparison of the 4 temperature distributions in Figure 28 that the mesh refinement has an impact in the temperature distribution through the Z axis. The results are clearly dependent on the mesh when Mesh 0 and Mesh 1 are being used, since those results differ from the ones obtained with Meshes 2 and 3.

There is no difference between Mesh 2 and 3, which is why the lines in the graph overlap. Mesh 3 is not visible in Figure 28. This means that refining more than what it was done in Mesh 2 makes no sense, since results will not improve and computational times will increase.

6.3.4.3 Graphs through the X axis

Graphs for the temperature distribution on the X axis have been done as well. Figure 29 shows the plotting line through the X axis, at Z = 32 cm.

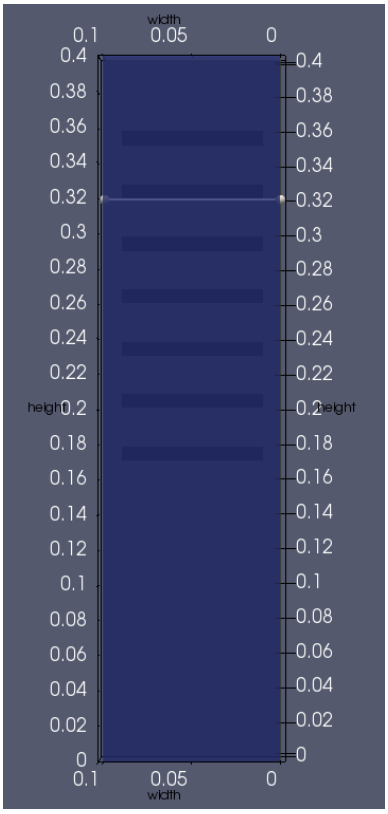

Figure 29 - X axis plot lines at Z = 32 cm

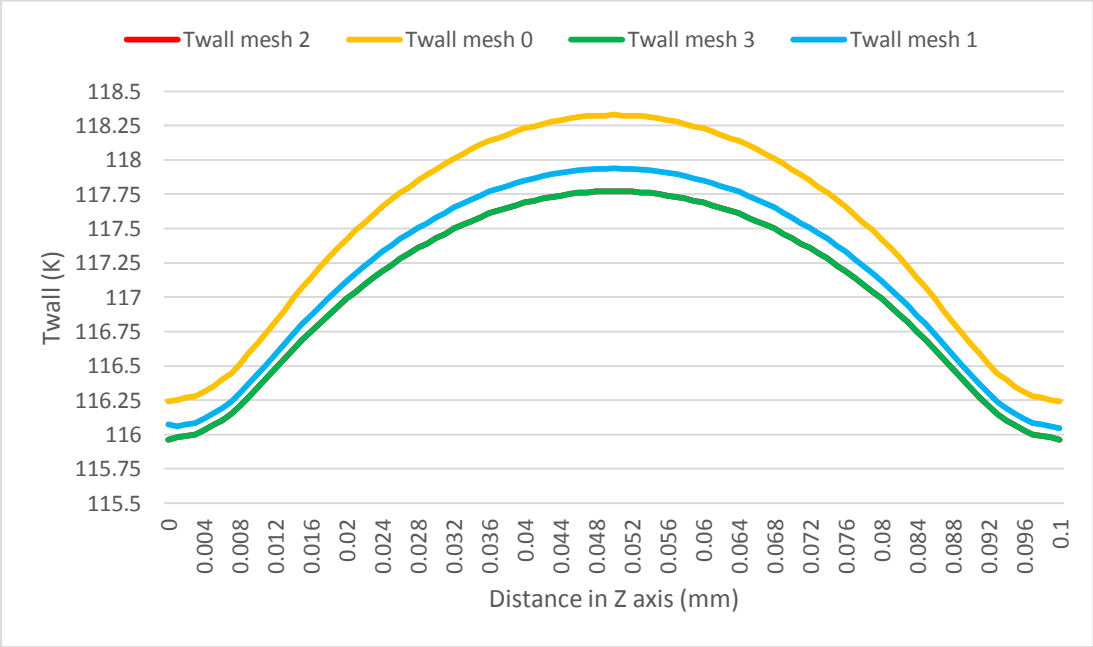

Figure 30 - X axis wall temperatures

Figure 30 shows the temperature distributions for each mesh, through the X axis at the height of Z = 32 cm. The results are close to the ones obtained in Figure 28, showing that there is improvement when refining the mesh up until Mesh 2. It is proven that Mesh 2 and Mesh 3 provide the same results.

6.3.4.4 Mesh assessment conclusions

Figures 28 and 30 show that the variation on the number of cells in the mesh has an impact on the results that are obtained when measuring temperatures through the hot aluminium wall. It can be seen that there is a difference between Mesh 0, Mesh 1 and Mesh 2. However, it is proven that using Mesh 3 does not provide better results.

Therefore, due to the fact that there is no difference between Meshes 2 and 3, it is concluded that using Mesh 2 is the best option in order to try to optimize the computation time while obtaining the best possible results at the same time.

6.4 Study 1 conclusions

The outlet temperature result is close to the measured values. As it has been previously stated, this difference could be explained by the fact that the real experimentation didn't measure the outlet temperature in the channel outlet itself, but in the outlet bath instead (a few centimeters afterwards). There might be some energy losses in this distance, which might induce to lower measured values. Moreover, since the thermocouples have 1ºC of measurement uncertainty, this is considered as a good result. This positive result shows that the water channel has received the same amount of energy as in the real experiment.

Once the water starts boiling vigorously, this simulation clearly doesn't work for wall temperatures, as the results from the thermocouples' locations show. Due to the fact that a simulation for single phase was done, the water isn't able to boil and therefore wall temperatures rise too much. The difference between the simulated values and the experimental ones show how q''_{wall} has been distributed in the fluid. While q''_{wall} is distributed in 3 ways for 2 phase flow, it is only transmitted through convection in single phase.

Single phase flow:

$$q''_{wall} = q''_{convection} \tag{6.1}$$

Two-phase flow:

$$q''_{wall} = q''_{convection} + q''_{evaporation} + q''_{quenching} \tag{6.2}$$

Therefore, the temperature difference between experimental and simulated results gives an idea of the amount of heat flux that was absorbed by $q''_{evaporation} + q''_{quenching}$ in the real experiment.

The assessment of q''_{wall} differs from hypothesis done by ABB. ABB's approximation was that the amount of heat flux that would come from the heaters could be simplified as $q''_{wall\ ABB\ approximation} = 5\ \frac{W}{cm^2}$, applied to the heated area that they defined.

The results obtained in the simulation show that the heat is actually spread through the whole aluminium block, obtaining values in the range of ≈2,5 W/cm^2 in the thermocouples.

7 Study 2: single phase flow with nucleate boiling conditions

The aim for this simulation was to acquire data for the nucleation sites that were reported in ABB's report, and compare the results that they obtained to the ones obtained through our simulation. The position of those nucleation sites is shown in Figure 17.

7.1 Case set up

The case set up remains the same from the previous simulation. The model remains the same, only changing some of the parameters that are included in section 6.1.1. Therefore, the case setup is not presented again.

7.1.1 Flow conditions

The flow conditions have been slightly modified for this study. Both the channel mass flux and the heat applied to the heaters were reduced in the experiment to ensure sub-nucleate boiling conditions.

The following list shows the variables used in this simulation.

$T_{in} = 90ºC$

$\mathrm{G} = 58.06\ \frac{kg}{m^2 s}$

$\mathrm{q}'' = 3\ \frac{W}{cm^2}$

$p = 1\ atm$

$\rho_{l\ inlet} = 965 \frac{kg}{m^3}\ (1\ atm, 90ºC).$

$A_{channel} = 3x100mm^2 = 0.0003m^2$

$$U_{in} = \frac{G}{\rho_{l\ inlet}} = \frac{58.06\ \frac{kg}{m^2 s}}{962\ \frac{kg}{m^3}} = 0.0601 \frac{m}{s}$$

$$\overline{C_p} = \frac{h_{out} - h_{in}}{T_{out} - T_{in}} = \frac{406450 - 376990}{97 - 90} = 4208.57 \ \frac{J}{kg \cdot K}$$

$$\mu_{in} = 0.3144 \ x \ 10^{-3} \ Pa \cdot s$$

7.1.2 Expected results

No experimental results for this run regarding outlet or thermocouple's temperature were reported for this run. Therefore, there is no data to match the simulation's results.

7.1.3 Q applied to the heaters

The heated area that was mentioned in Kromer's report was used in order to calculate the amount of heat that should be applied in the heaters, taking into account that the model has no heat losses.

$$Q_{heaters} = q'' \cdot A_{heated} = 3 \ \frac{W}{cm^2} \cdot 203.2 \ cm^2 = 609.6 \ W \tag{7.1}$$

7.2 Simulation results

The results for this simulation will not vary much from the ones obtained in Study 1, since it's the same model with some variations in the inlet parameters.

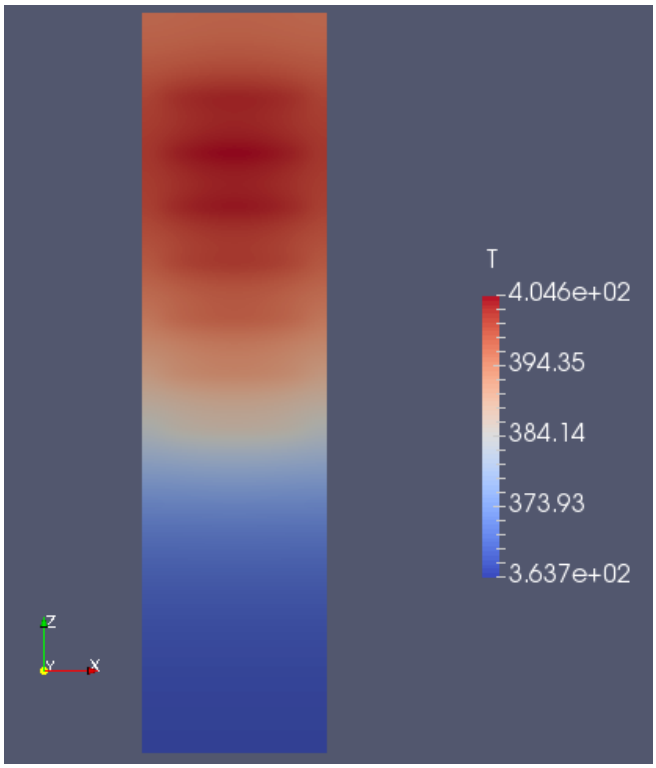

Figure 31 - Temperature distribution in aluminium block, Study 2. Temperature in K

Figure 31 shows a temperature distribution in the aluminium block, which is really similar to the one obtained for Study 1. The only difference is that the temperature values are lower, since the heat input in the heaters is lower as well.

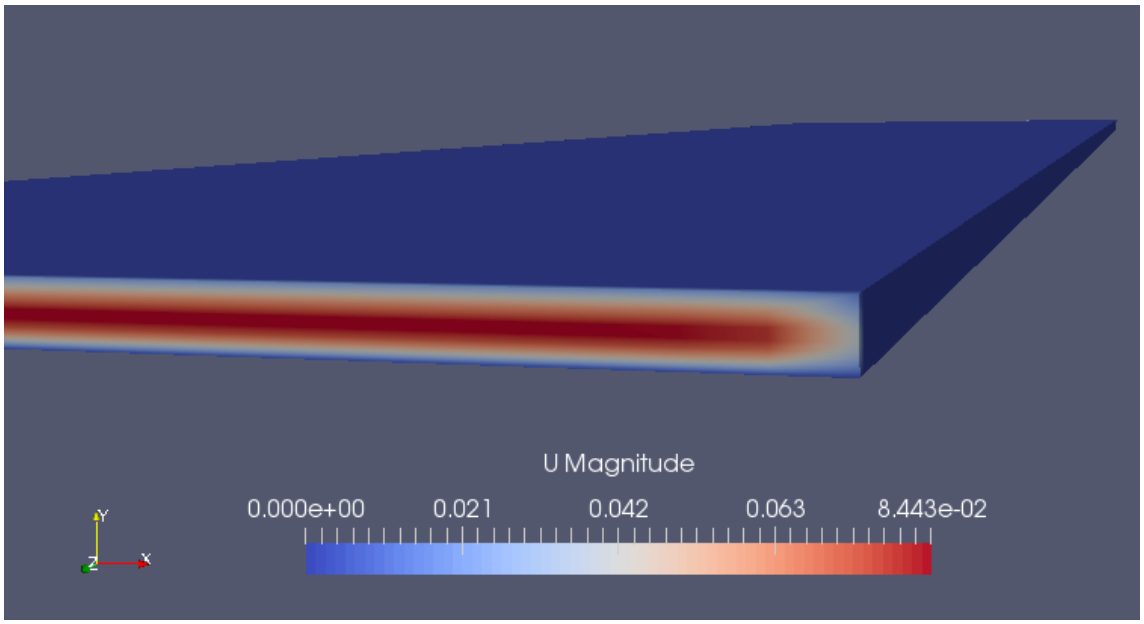

Figure 32 - Water velocity profile in the outlet, Study 2. Velocity in m/s

Despite the fact that the water velocity is lowered, it can be seen in Figure 32 that the water velocity profile is attained in the outlet. It is proven as well that the non-slip boundary conditions for the fluid velocity are being respected, since the velocity of the water in the walls is equal to 0.

Given that the water velocity and the temperature distribution seemed to behave properly, the results were taken into account as correct and therefore the model was used for further measurements, which are explained in the following sections.

7.2.1 Heat flux and temperature measurements for nucleation sites' location

The table below shows the results obtained for this Study. Temperature is shown in ºC, q'' in W/cm^2 and positions in m.

q'' through the wall is calculated for each nucleation site. Both calculations from the aluminium block and the water channel are included, using the formula that was presented in section 5.5.4.

Y coordinate for the nucleation sites is not included, due to the fact that it's fixed (located in the aluminium wall). The value for Y in this simulation is Y = 0.023m.

Nuc. Site #	x position	z position	wall temp.	q'' nucleation site Al	q'' nucleation site water
1	0.0521	0.21	119,24506	2,553552	2,553404589
2	0.0555	0.2078	119,08858	2,59578	2,595680108
3	0.063	0.2068	118,77761	2,627244	2,629555665
4	0.0547	0.2037	118,26041	2,676924	2,677106434
5	0.0526	0.203	118,28701	2,679684	2,679642965
6	0.0599	0.2003	117,22572	2,597712	2,597610077
7	0.0537	0.2001	117,27826	2,60268	2,602756662
8	0.0499	0.1993	117,04679	2,579496	2,579670553
9	0.06	0.2135	119,47634	2,478756	2,478632062
10	0.0659	0.2132	119,21178	2,469648	2,469625539
11	-	-	-	-	-
12	-	-	-	-	-
13	0.0659	0.2014	117,54715	2,625036	2,624868597
14	0.0664	0.1988	116,52928	2,527056	2,527212148
15	0.0463	0.1996	117,02075	2,577012	2,57709726

Table 2 - Nucleation Sites results

7.2.2 Sensitivity analysis

Given that the author was not supplied with experimental results, it hasn't been possible to assess the credibility of the simulation results. In order to assess the obtained data, a sensitivity analysis was done, changing the amount of heat that is applied to the heaters by 5%. The second study was used for this case, and thus the used heat values are $Q_{-5\%} = 579{,}12\ W$ and $Q_{+5\%} = 640{,}08\ W$.

The data for nucleation sites was obtained for each simulation. The following sections show the results for both cases, as well as a result comparison in order to assess the sensitivity of the case.

7.2.2.1 Results for Q +5%

Nuc. Site #	x position	z position	wall temp.	q'' nucleation site Al	q'' nucleation site water
1	0.0521	0.21	120,67884	2,681064	2,68105828
2	0.0555	0.2078	120,51453	2,7255	2,72546595
3	0.063	0.2068	120,18801	2,761104	2,76101415
4	0.0547	0.2037	119,64495	2,81106	2,81093602
5	0.0526	0.203	119,67289	2,813544	2,8136196
6	0.0599	0.2003	118,55854	2,727432	2,72748782
7	0.0537	0.2001	118,6137	2,732952	2,73289174
8	0.0499	0.1993	118,37066	2,708664	2,70864765
9	0.06	0.2135	120,92168	2,60268	2,60255448
10	0.0659	0.2132	120,64389	2,593296	2,59310682

11					
12					
13	0.0659	0.2014	118,89604	2,756136	2,75612489
14	0.0664	0.1988	117,82727	2,653464	2,65356081
15	0.0463	0.1996	118,34331	2,705904	2,70592731

Table 3 – Nucleation sites results for Q+5%

7.2.2.2 Results for Q -5%

Nuc. Site #	x position	z position	wall temp.	q'' nucleation site Al	q'' nucleation site water
1	0.0521	0.21	117,81118	2,425764	2,42571414
2	0.0555	0.2078	117,66253	2,465784	2,46589426
3	0.063	0.2068	117,36711	2,498076	2,49806042
4	0.0547	0.2037	116,87577	2,543064	2,54324008
5	0.0526	0.203	116,90104	2,545824	2,54564795
6	0.0599	0.2003	115,89282	2,467716	2,46771395
7	0.0537	0.2001	115,94272	2,472684	2,47260321
8	0.0499	0.1993	115,72283	2,450604	2,45067508
9	0.06	0.2135	118,0309	2,354556	2,35469127
10	0.0659	0.2132	117,77957	2,346	2,34614426
11					
12					
13	0.0659	0.2014	116,19817	2,49366	2,4936123
14	0.0664	0.1988	115,2312	2,400648	2,40084511
15	0.0463	0.1996	115,69809	2,44812	2,44821207

Table 4 - Nucleation sites results for Q-5%

7.2.2.3 Sensitivity analysis comparison

Graphs are used in this section to ease the comparison between values obtained for the different heat values. Graphs for wall temperature and calculated heat flux are included, which correspond to Figures 33 and 34.

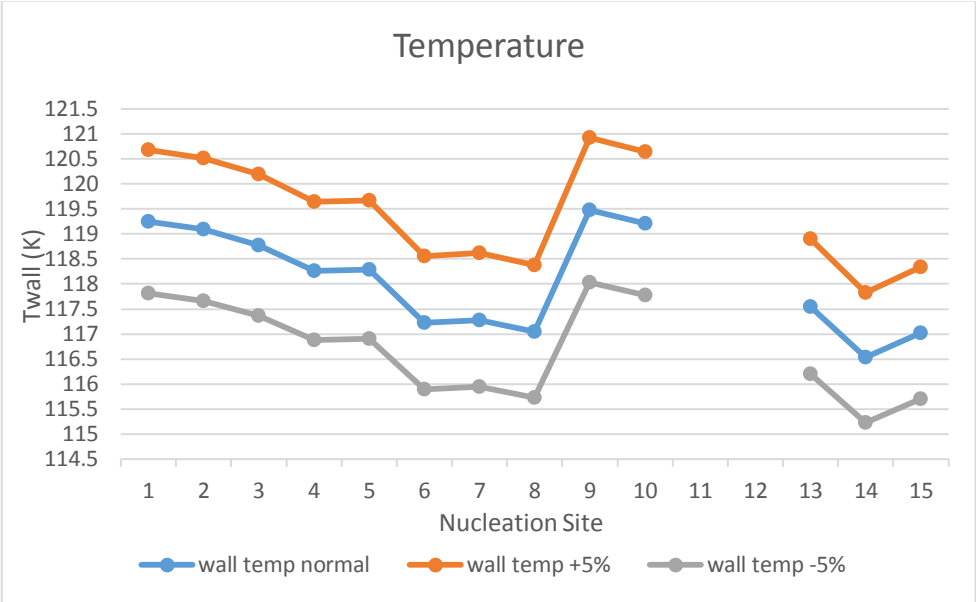

Figure 33 - Sensitivity analysis - Temperature

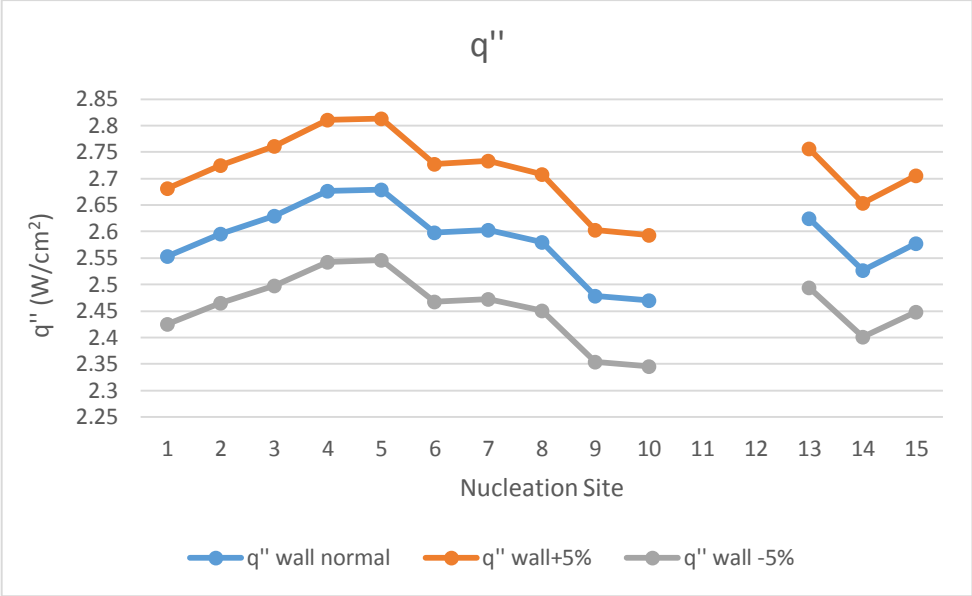

Figure 34 - Sensitivity analysis - Heat flux

The sensitivity analysis shows that the simulation is behaving properly. The results included in Figures 33 and 34 are varying in a linear way when the input values are incremented or decremented, which makes sense when taking into account the equations that are being used.

Given the case that those values would not behave linearly, it would mean that the equations would either not had been solved properly, or that they were written incorrectly. Therefore, this simple assessment ensures that this is running as it should.

7.3 Results comparison

Since there is no experimental results regarding the temperature outlet, only the heat assessment was done for this study.

Using the procedures described in section 5.5.1, the simulation shows the total amount of heat Q that is transferred to the water through the aluminium wall. In this case, it's a total of 603.3 W.

Given that the amount of heat applied to the heaters is 609.6 W, it is concluded that the model is adiabatic. As it has been explained before, the obtained error is caused by numerical errors, due to the fact that the aluminium wall has a huge area.

7.4 Study 2 conclusions

Given that no experimental results other than the nucleation sites' location were provided to the author, the results obtained in this study cannot be compared. Therefore, a sensibility analysis is performed in order to ensure the credibility of the obtained data.

The sensitivity analysis shows that the case is being solved properly, since the linearity of the result variation makes sense. It is thus believed that those results should therefore be taken into account as correct.

In addition, the adiabaticity assessment shows that the model has no heat losses other than the errors that take place due to numerical uncertainties, which are completely negligible. In fact, those errors can be explained when the results obtained for q'' calculated from the aluminium solid and from the wall are compared, which can be seen in table 2. A difference in the 4^{th} or 5^{th} decimal might not be significant for single value comparisons. However, when integrated through the huge area that the heated wall has, it creates the error that can be seen in the adiabaticity test.

8 Single phase conclusions

This section includes a summary of the main objectives that wanted to be achieved with single phase flow simulation, and intents to draw conclusions from the obtained results.

The first clear conclusion is that a model that simulates the real experiment has been created. Heat insulation has been proven, and the sensitivity analysis indicates that results behave properly. The mesh assessment indicates as well that a proper mesh has been used to obtain the results shown.

Conjugate heat transfer has been proven as well, since the calculated q'' values from both the water channel and the aluminium block are equal.

In addition, a system that eases the task to obtain data in any location of the heated wall has been implemented. It is believed by the author that this script will facilitate measurement tasks if it is decided to opt for the further improvement of this model.

However, it has been seen that wall and water temperatures rise too much, given the fact that single phase flow has been simulated in this case. It is the author's opinion that a heat flux partitioning should be implemented in the water part of the solver in order to acquire more realistic results. It might not be necessary to implement the whole bubble formation code. Making sure that the convection heat flux term of the water region doesn't increase more than what it's supposed to should be enough to obtain the right temperatures.

9 Modelisation of the experiment for the two phase simulation

This section includes the changes that have been done to the model for it to be able to be calculated using the two phase solver.

9.1 Simulation simplifications

In order to save computational times, the aluminium block and the heaters have not been included in this model. Hence, only the water channel is simulated in this study, which can be seen in Figure 35.

9.2 Mesh

As it has been stated in the previous section, the solid structures of the model have been omitted for this study. Therefore, only the mesh that models the water channel has been reproduced.

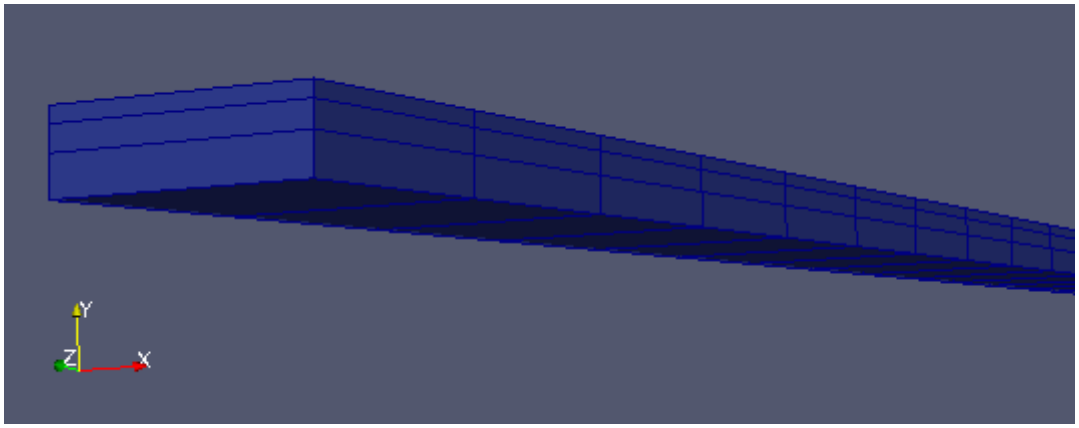

Figure 35 - Mesh for the two phase simulation

Figure 35 shows the mesh that was used for the two phase simulation, which consists of tetrahedral cells. In order to spare computational time, the number of cells in each direction has been notably reduced. In fact, the new mesh has 1 cell in the X direction, 3 in the Y direction and 50 in the Z direction.

It can be seen that the cell that is closest to the heated area is actually the widest one, which is contrary to the concept that was used in the previous mesh. This had to be done due to the incapability of the solver to calculate the case when the first cell was too small. This issue will be explained in further sections.

9.3 Boundary conditions

This study required a small change in the boundary conditions. Given that the aluminium block and the heaters were omitted from this model, the heat input needed to be set as a Boundary Condition in the boundary of the water that would be touching the aluminium wall. No other changes are done to any other boundaries.

10 Study 3: two phase flow

This study is the recreation of the experiment for two phase flow. Its main objective is to use the solver supplied by KTH in order to see if it's capable of solving the case, even though it's a solver that was designed for a highly turbulent flow. In order to achieve that, another model is created, which is presented in the following sections.

10.1 Case set up

This section includes the different set up concepts that are part of Study 3. The hypothesis for this study have been included in section 3.2

10.1.1 Flow conditions

Since this simulation is trying to assess the bubble formation, the inlet parameters are maintained from Study 2.

$T_{in} = 90ºC$

$\mathrm{G} = 58.06\ \frac{kg}{m^2 s}$

$\mathrm{q}'' = 3\ \frac{W}{cm^2}$

$p = 1\ atm$

$\rho_{l\ inlet} = 965 \frac{kg}{m^3}\ (1\ atm, 90ºC).$

$A_{channel} = 3x100mm^2 = 0.0003m^2$

$$U_{in} = \frac{G}{\rho_{l\ inlet}} = \frac{58.06\ \frac{kg}{m^2 s}}{962\ \frac{kg}{m^3}} = 0.0601 \frac{m}{s}$$

$$\overline{C_p} = \frac{h_{out} - h_{in}}{T_{out} - T_{in}} = \frac{406450 - 376990}{97 - 90} = 4208.57\ \frac{J}{kg \cdot K}$$

$$\mu_{in} = 0.3144\ x\ 10^{-3}\ Pa \cdot s$$

10.1.2 Expected results

No experimental results for this study regarding the outlet or thermocouple's temperature were reported in the experimental report. Therefore, there is no data to match the simulation's results.

10.2 Results and discussion

Figure 36 represents the last iteration obtained when the solver was solving the two phase simulation. It shows the exact iteration before the simulation crashes.

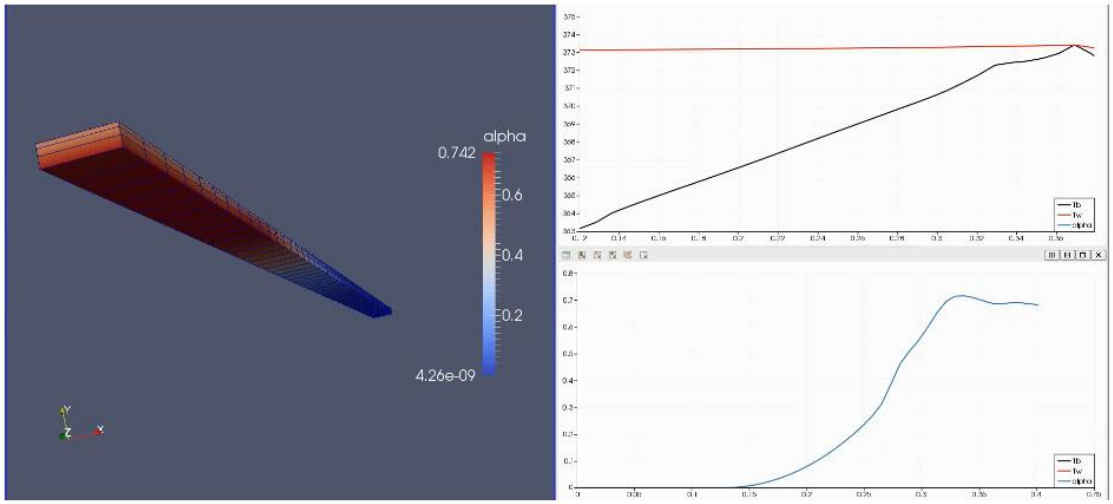

Figure 36 – Study 3 results

In Figure 36, the picture on the left shows the void volume fraction distribution among the water channel (alpha). The graphs on the right side of the picture show some variables. The upper graph shows the water temperature and the heated wall temperature, and the other graph shows alpha. The X axis stands for the length of the channel.

It can be seen that results make sense for alpha and for the water temperatures, but don't really make sense for the wall temperatures. The reason why this solver crashes is because the water temperature surpasses the temperature value of the wall, which is physically impossible.

This occurs due to the fact that the superheat temperature (T_{sup}) isn't being properly calculated, as well as other boiling parameters that depend on that value. T_{sup} should be

around 13-15 ºC in the area where nucleate boiling occurs, while the simulation gives 0.2-0.4ºC as result. Given the fact that the wall temperature is updated in the solver as:

$$T_{wall} = T_{sat} + T_{sup} \tag{10.1}$$

This means that the wall temperature is never calculated properly. Since water temperature is being calculated correctly, it will eventually surpass the saturation temperature once the water starts boiling vigorously, and there's where the error takes place.

The main reason why T_{sup} is not being calculated properly is because this solver is highly dependant on the value of the adimensional distance where the water flow changes from laminar to turbulent, also known as y^+. The creator of the solver specifies that this value must be higher than 30 in the cells that are closer to the wall, so the calculations are done properly. T_{sup} and other boiling parameters depend on that factor, which is calculated as follows:

$$u_{fw} = \sqrt{\frac{\tau(y)}{\rho}} = \sqrt{\frac{\frac{\partial u}{\partial y}|_{y=0}\,\mu}{\rho}} \tag{10.2}$$

$$y^+ = \frac{y\,u_{fw}}{\nu} \tag{10.3}$$

It can be seen that y^+ depends on the velocity of the fluid and the distance of the first cell center closer to the wall. This means that the solver is highly mesh dependent and it also depends on the velocity of the fluid.

Given that the channel that is being simulated is extremely narrow and that the fluid velocity is really low, it's technically impossible to obtain $y^+ > 30$. When comparing to the simulation for which this solver was meant to be used, it can be seen that the fluid channel was 3 times wider and, which is more important, the fluid velocity was 30 to 40 times higher, depending on the run that was being simulated. That made the simulated flow extremely turbulent, and therefore presented huge differences from the ones used in this study.

10.3 Study 3 conclusions

The main conclusion that can be extracted from this study is that the used solver was not created to simulate this kind of flow. Most of the parameters (as it can be seen in equations 10.2 and 10.3) depend on the conditions of the flow, which present too many differences from the one that was originally used for it to work on our simulation.

However, even though the obtained results are just transient solutions (since the steady state solution cannot be reached), it can be seen that they are logical in terms of alpha and water temperature. The void fraction starts increasing where the nucleation sites were located (study 2), which makes sense. This means that alpha was calculated properly, i.e. the enthalpy transmission and the phase change calculations in the liquid are correct. The simulation crashes due to other factors that make it impossible for the solver to keep going.

The solver also shows a clear case of huge mesh dependence. From what it can be seen in this case, the results will vary in relation to the distance from the first cell center to the wall.

There is clearly a lot of work to do in the two phase case. At least, it could be seen that this solver was unable to do the job.

11 Environmental impact

Given that the entirety of this study has been developed in a single personal computer, the environmental impact produced by its energy consumption is clearly negligible. However, it can be noted that large data centers like the ones used at KTH are huge energy consumers, and therefore may act as notable actors in terms of environmental impact.

In order to diminish those effects, many R&D projects have been done in the past years, which mainly focus on reducing the energy consumption of the data center, switch that consumption to electricity created by renewable energy sources, and optimizing its refrigeration system. One example of these projects is DC4cities[15], a project in which the author of this thesis was involved during his internship.

Another point of view that could be taken into account in this section could be the scenario of not performing this kind of studies, meaning that the boiling events in a nuclear reactor would not be studied using simulations. As it has been stated during this project, boiling is a huge actor in terms of heat transfer through water, and therefore, the good functioning of nuclear reactors is clearly dependent on it. Given the fact that nuclear reactors could be potentially dangerous for the environment in case of an accident, it is clear that this kind of studies are extremely beneficial.

To summarize, it is concluded that the energy consumption of the simulations that have been done in this study have no environmental impact, and in addition, the benefits of doing it are indeed beneficial for the environment.

12 Budget

This project has been performed during an internship at KTH, which has supposed some manteinance costs for the author that are taken into account in this budget. That value is estimated from the monthly expenses of the author.

In addition, an estimation of the energy consumption and its cost is included as well. The computer is supposed to be on 24 hours a day for the 6 months of the internship (≈4320 hours), and its energy cost is fixed at 0.12906 €/kWh, which is considered to be the average fixed price for domestic consumption.

Concept	Quantity	Cost
Maintenance costs	1100€/month x 6 months	6.600 €
Computer energy consumption	300 W x 4320 h x 0.12906 €/kWh	167,26 €
Total		6.767,26 €

Table 5 - Project budget

The budget that is represented in Table 5 shows that most of the project costs are related to the maintenance of the student, and points out that the energy consumption cost is not extremely high, if it is taken into account that the computer has been working for 6 months straight.

In terms of the maintenance costs, the author would like to thank the Argos professorship, which provided with a scholarship that was crucial for the author to be able to complete the 6 months stay in Sweden.

13 Final conclusions and future steps

In order to summarize the conclusions obtained from the work done for this Thesis, main objectives of this thesis are presented again.

The author has successfully comprehended the physical phenomena that occur when water is boiling and has explained them in section 3, presenting the different equations that need to be used for each concept.

OpenFOAM is the CFD environment that has been used in order to perform the simulations, among all the other possibilities. The reasoning for this decision is presented in section 4. The fact that OpenFOAM is open software and that its solvers are easily modifiable have been the key points for choosing this option.

Various studies have been done in order to try to recreate the real experiment. The first approach to do so is to use a single phase multi-region solver that is included in OpenFOAM, called *chtMultiRegionFoam*. This part of the study determined that the heat transfer is done properly through the different regions of the model, and that the boundary conditions and water velocity profiles are working properly. However, the fact that boiling is not being taken into account affects the temperature results, making them much higher than what they should be.

Then, another study was done in order to develop a tool that could gather information in nucleation sites in an automatic and easy way. This could be really useful in further improvements of the model.

Finally, the two phase solver that was designed for a highly-turbulent case was used. A new model was designed, and many issues were encountered. Even though the simulation could not be run until its convergence to the steady state, the causes for its errors were found and discussed.

In regards of the further steps, it is clear that using OpenFOAM's new solver *reactingTwoEulerFoam* to calculate the water flow is the way to go. However, as it has been explained in section 4.4, some equations need to be included in that solver for it to properly calculate boiling. Once this is done, the resulting solver should be implemented to *chtMultiRegionFoam*, for it to be able to simulate both the regions and the water channel, and thus calculate the heat transfers from the heaters towards the water, as it has been done in studies 1 and 2 in this thesis.

Taking all that information into account, it is believed by the author of this Master's Thesis that, even though there is a lot of work to be done regarding the simulation of nucleate boiling, this study represents a key step and has provided with the required overview to efficiently fulfill following studies.

14 References

[1] Heiko Kromer. *Experimental Determination of Model Parameters for Subcooled Nucleate Flow Boiling in a Minichannel*. (Institut National des Sciences et Techniques Nucleáires, Stockholm, 2015)

[2] Henryk Anglart. *Thermal Hydraulics in Nuclear Systems.* (KTH, Stockholm, 2008)

[3] T. Hibiki and M. Ishii. *Development of one-group interfacial area transport equation in bubbly flow systems.* (International Journal of Heat and Mass Transfer, 45:pp. 2351-2372, 2002).

[4] A. Tomiyama. *Struggle with computational bubble dynamics.* (Third International Conference on Multi-phase flow, 2008)

[5] A. Ghione. *Development and validation of a two-phase CFD model using OpenFOAM* (KTH, Stockholm, 2012).

[6] E. Michta. *Modeling of Subcooled Nucleate Boiling with OpenFOAM.* (KTH, Stockholm, 2011)

[7] https://openfoamwiki.net/index.php/Main_Page

[8] chtMultiRegionFoam wiki [https://github.com/OpenFOAM/OpenFOAM-2.4.x/tree/master/applications/solvers/heatTransfer/chtMultiRegionFoam]

[9] L. Schiller and Z. Naumann. *A drag coefficient correlation.* Z. Ver. Deutsch. Ing., 77:318, 1935.

[10] M. Ishii and N. Zuber. *Drag coefficient and relative velocity in bubbly, droplet or particulate flows*. AIChE J., 25:843, 1979

[11] C.Y. Wen and Y.H. Yu. *Mechanics of fluidization.* Chemical Engineering Progress Symposium Series, 62:100, 1966.

[12] OpenFOAM user guide [http://foam.sourceforge.net/docs/Guides-a4/UserGuide.pdf]

[13] reactingEulerFoam wiki [https://github.com/OpenFOAM/OpenFOAM-3.0.x/tree/master/applications/solvers/multiphase/reactingEulerFoam/reactingTwoPhaseEulerFoam]

[14] Lway Al-Maeeni. *Sub-cooled nucleate boiling flow cooling experiment in a small rectangular cannel.* (KTH, Stockholm, 2015)

[15] Gas Natural Fenosa – Proyecto DC4cities [http://www.gasnaturalfenosa.com/es/actividades/innovacion/modelo+de+innovacion/proyectos/eficiencia+energetica/1297293935421/dc4cities.html]